Supporting Information

A red fluorescence '*off-on*' molecular switch for selective detection of Al^{3+}, Fe^{3+} and Cr^{3+}: experimental and theoretical studies along with living cell imaging

Shyamaprosad Goswami,[*a] Krishnendu Aich,[a] Sangita Das,[a] Avijit Kumar Das,[a] Deblina Sarkar,[b] Sukanya Panja,[c] Tapan Kumar Mondal,[b] Subhra Kanti Mukhopadhyay[c]

[a]Department of Chemistry, Bengal Engineering and Science University, Shibpur, Howrah 711103, West Bengal, India E-mail: spgoswamical@yahoo.com

[b]Department of Chemistry, Jadavpur University, Jadavpur, Kolkata, India

[c]Department of Microbiology, The Burdwan University, Burdwan, India.

1. General

Unless otherwise mentioned, materials were obtained from commercial suppliers and were used without further purification. Thin layer chromatography (TLC) was carried out using Merck 60 F_{254} plates with a thickness of 0.25 mm. Melting points were determined on a hot-plate melting point apparatus in an open-mouth capillary and are uncorrected. ^{1}H and ^{13}C NMR spectra were recorded on JEOL 400 MHz and Brucker 500/300 MHz instruments and mentioned below (figure caption) the NMR spectra. For NMR spectra, $CDCl_3$ was used as solvent using TMS as an internal standard. Chemical shifts are expressed in δ units and ^{1}H–^{1}H and ^{1}H–C coupling constants in Hz. UV-vis spectra were recorded on a JASCO V-630 spectrometer. Fluorescence spectra were recorded on Perkin Elmer LS 55 fluorescence spectrometer. FT-IR spectrum was recorded on a JASCO FT/IR-460 plus spectrometer, using KBr disc. CHN analysis was performed with CHN analyzer (2400 series II). For the titration experiment we use the cations viz. [Na^{+}, K^{+}, Ca^{2+}, Ni^{2+}, Mn^{2+}, Zn^{2+}, Cd^{2+}, Cu^{2+}, Fe^{3+}, Cr^{3+}, As^{3+}, Pb^{2+}] as their chloride salts and Al^{3+}, Bi^{3+} as their nitrate salts.

2. Synthetic method for the preparation of the probe (SBPQ):

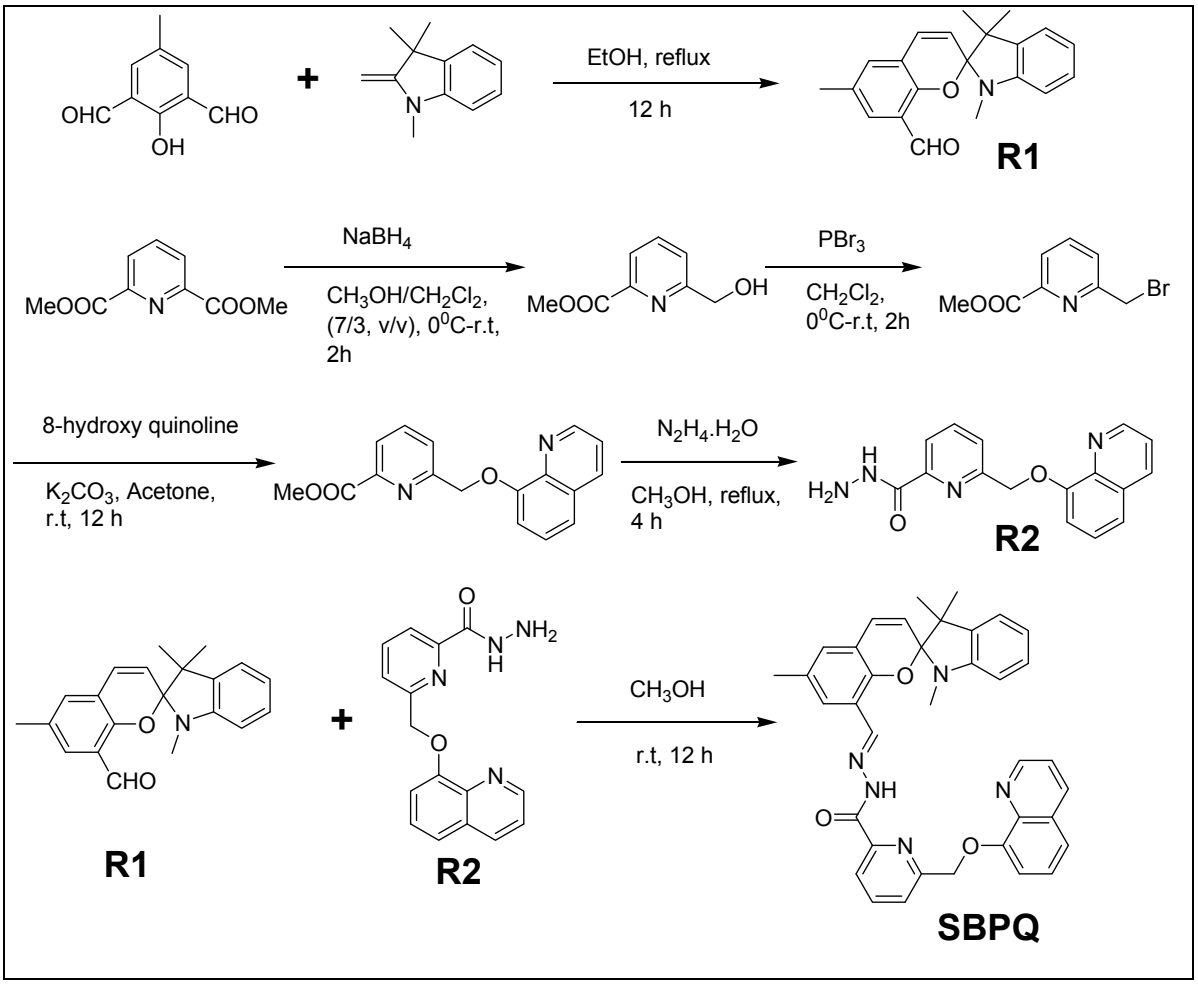

Scheme 1: Synthetic strategy of SBPQ

Synthesis of compound R1:

To the stirred solution of 4-methyl-2,6-diformyl phenol (0.5 g, 3.0 mmol), dissolved in 30 ml ethanol, was added drop-wise 1,3,3-trimethyl-2-methyleneindoline (0.53 g, 3.0 mmol), dissolved in another 20 ml ethanol, during 1h time period. The reaction mixture was then stirred for 12 h under refluxing condition. The solvent was evaporated under reduced pressure and the crude product was purified through silica gel (100-200, mesh size) column chromatography using 2-3% ethyl acetate in petroleum ether as eluent to afford **R1** (0.65 g, yield = 67%) as brownish yellow oil.

^{1}H NMR (400 MHz, $CDCl_3$): δ 1.165 (s, 3H), 1.285 (s, 3H), 2.300 (s, 3H), 2.739 (s, 3H), 5.778 (d, *J* = 8 Hz, 1H), 6.515 (d, *J* = *6.4* Hz, 1H), 6.844 (m, 2H), 7.069 (dd, *J*= 10.8 Hz, 2H), 7.159 (dd, *J* = 6.4 Hz, 1H), 7.439 (s, 1H), 10.114 (s, 1H).

^{13}C NMR (100 MHz, $CDCl_3$): δ 20.359, 20.505, 28.885, 29.043, 52.095, 105.531, 107.028, 119.619, 120.070, 120.444, 121.502, 122.311, 127.457, 127.760, 128.907, 129.381, 133.609, 136.424, 147.872, 155.652, 189.131.

ESI-MS: calculated for $C_{21}H_{22}NO_2$ $[M + H]^+$ (m/z): 320.1651 ; found: 320.2144.

Elemental Analysis: calculated (C, 78.97; H, 6.63; N, 4.39); found (C, 78.54; H, 6.25; N, 4.24).

Synthesis of the probe (SBPQ):

Compound R1 (0.5 g, 1.56 mmol) was dissolved in 20 ml dry methanol and compound R2 (0.45 g, 1.57 mmol) was added to it. The whole reaction mixture was stirred for 12 h at room temperature. The solvent was evaporated under reduced pressure and the crude product was purified through silica gel (100-200, mesh size) column chromatography using 20 - 40% ethyl acetate in petroleum ether as eluent while the SBPQ obtained as off-white solid. The solid obtained was dissolved in minimum volume of dichloromethane solution and re-precipitated using pentane. Filtered the precipitate and dried under vacuum, which afford a better purified white colored compound (yield = 62%).

Mp = (> 300^{0}C, decomposed).

^{1}H NMR (400 MHz, $CDCl_3$): δ 1.285 (s, 3H), 1.332 (s, 3H), 2.290 (s, 3H), 2.768 (s, 3H), 5.558 (s, 2H), 5.706 (d, *J* = 8.4 Hz, 1H), 6.527 (d, *J* = 6.4 Hz, 1H), 6.759 (t, *J* = 11.6 Hz, 1H), 6.833 (d, *J* = 8 Hz, 1H), 6.934 (s, 1H), 7.019 (d, *J* = 6 Hz, 1H), 7.065 (d, *J* = 9.6 Hz, 1H), 7.111 (t, *J* = 6.4 Hz, 1H), 7.399 (t, *J* = 6.4 Hz, 1H), 7.448 (d, *J* = 6.4 Hz, 1H),

7.495 (t, *J* = 3.2 Hz, 1H), 7.779 (d, *J* = 6.4 Hz, 1H), 7.846 (t, *J* = 6.4 Hz, 1H), 7.889 (s, 1H), 8.193 (m, 2H), 8.287 (s, 1H), 9.000 (q, *J* = 2.4 Hz, 1H), 10.863 (s, 1H).

^{13}C NMR (100 MHz, $CDCl_3$): δ 20.41, 20.64, 20.83, 26.19, 28.98, 29.82, 52.05, 71.20, 105.00, 106.81, 110.18, 119.16, 119.59, 120.65, 121.77, 121.99, 122.21, 124.62, 126.75, 127. 47, 127.77, 129.29, 129.77, 129.97, 136.30, 136.77, 138.58, 140.38, 143.49, 148.13, 148.92, 149.64, 151.30, 153.88, 156.19, 160.07, 174.77

ESI-MS: calculated for $C_{37}H_{33}N_5O_3$ $[M + H]^+$ (m/z): 596.2662; found: 596.2659.

Elemental Analysis: calculated (C, 74.60; H, 5.58; N, 11.76); found (C, 74.54; H, 5.61; N, 11.31).

Synthesis of the Al^{3+} complex of SBPQ (SBPQ-Al):

SBPQ (50 mg, 0.08 mmol) and Al $(NO_3)_3$ (32 mg, 0.085 mmol) were mixed together and dissolved in 5 ml of methanol. After refluxing for 12 hours the reaction mixture was cooled at room temperature. A red coloured precipitate appeared and was filtered and dried in vacuum.

IR (cm^{-1}): 1114, 1385, 1521, 1627

ESI-MS: calculated for $C_{37}H_{35}AlN_5O_4$ $[M+Al^{3+}+H_2O]^+$ (m/z): 640.2482; found 640.2118.

3. General method of UV-vis and fluorescence titration:

By UV-vis method

For UV-vis titrations, stock solution of the receptor (20 μM) was prepared in [(CH_3CN / water), 1:1, *v/v*] (at 25°C) using HEPES buffered solution. The solutions of the guest cations using their chloride/nitrate salts in the order of 2×10^{-4} M, were prepared in deionized water using HEPES buffer at pH = 7.4. Solutions of various concentrations containing the sensor and increasing concentrations of cations were prepared separately. The spectra of these solutions were recorded by means of UV-vis method.

By fluorescence method

For fluorescence titrations, stock solution of the sensor (20 μM) was prepared in the same way as in the case of UV-vis titration. The solutions of the guest cations using their chloride/nitrate salts in the order of 2×10^{-4} M, were prepared in deionised water. Solutions of various concentrations containing sensor and increasing concentrations of cations were prepared separately. The spectra of these solutions were recorded by means of fluorescence method.

4. Effect of pH:

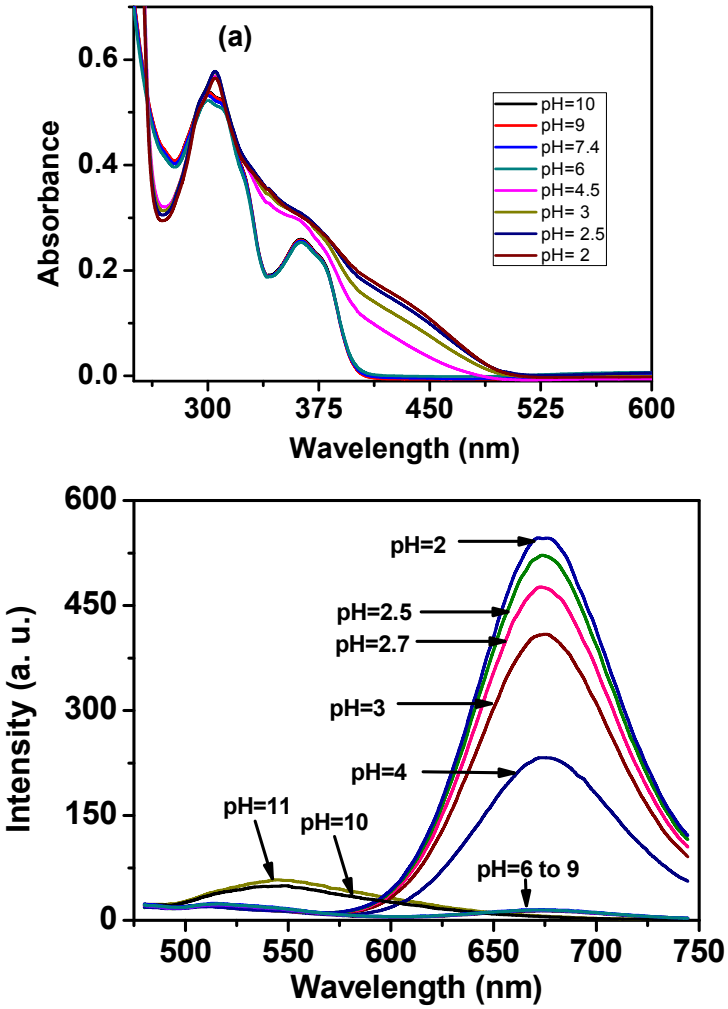

Figure S1: Plot of (a) absorption and (b) emission spectra of SBPQ (20 μM) upon variation of pH in CH_3CN-H_2O (1/1, v/v) solution, pH is adjusted by using aqueous solutions of 1 M HCl or 1 M NaOH.

5. Emission titration spectra of SBPQ :

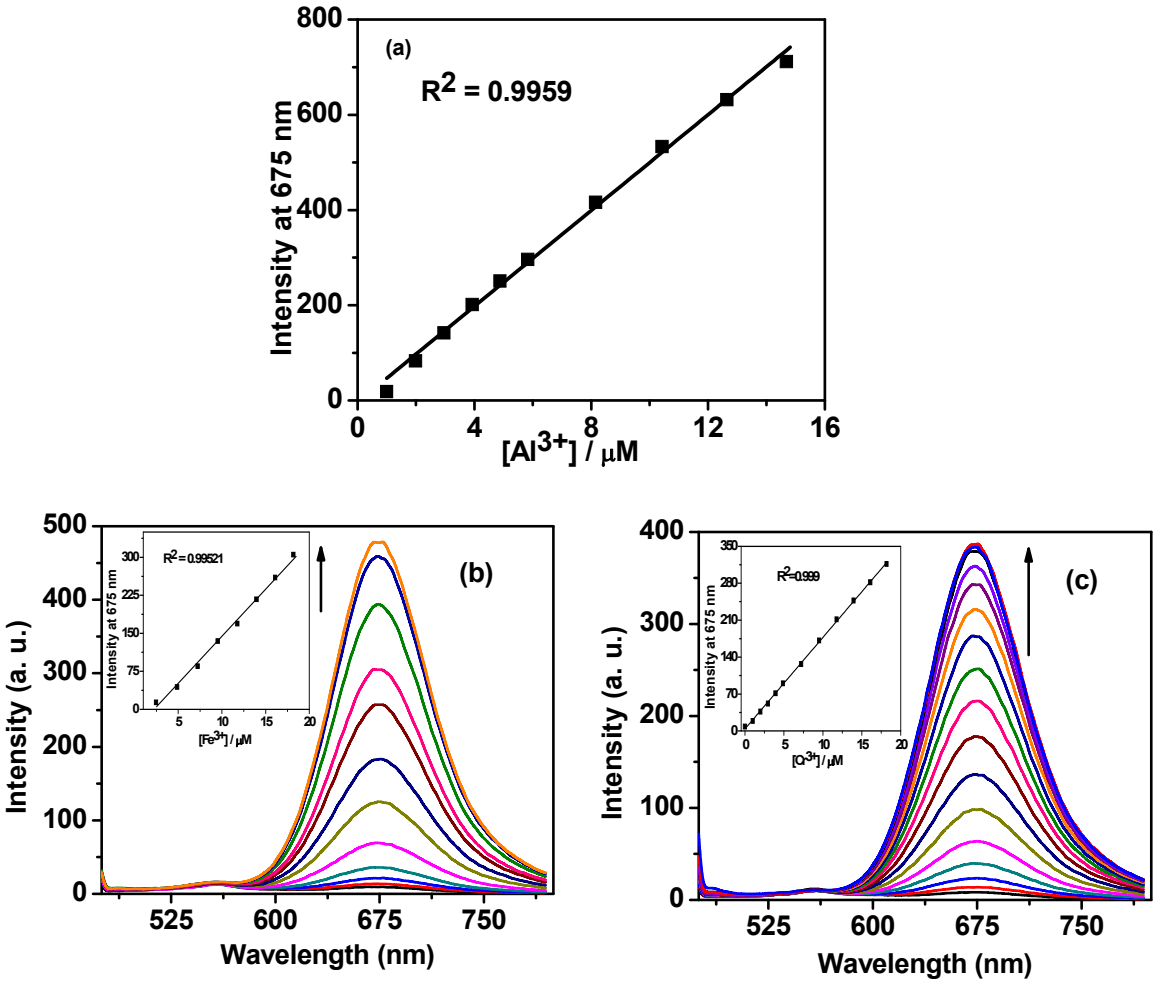

Figure S2: (a) The linear response curve of emission intensity of SBPQ at 675 nm depending on the Al^{3+} concentration. Change of emission spectra of SBPQ (20 μM) upon gradual addition of (b) Fe^{3+} and (c) Cr^{3+} (0 to 2 equivalents) in CH_3CN-HEPES buffer solution (1/1, v/v). Inset: Linear response curve of emission intensity of SBPQ with concentration of Fe^{3+} and Cr^{3+}. λ_{ex} = 460 nm.

6. UV-vis titration spectra of SBPQ with Al^{3+}, Fe^{3+} and Cr^{3+}:

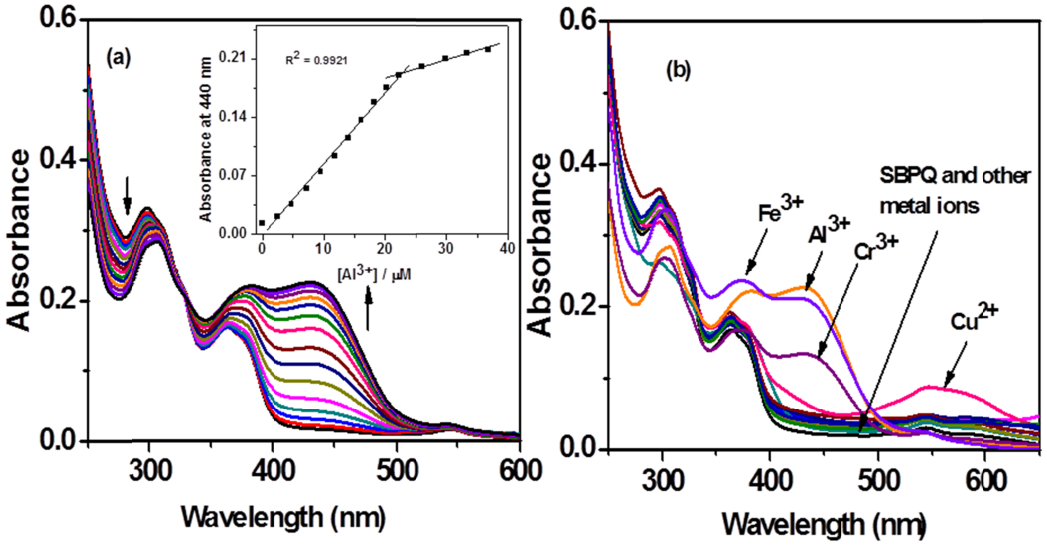

Figure S3: Change of absorption spectra of (a) SBPQ (20 μM) upon gradual addition of Al^{3+} (0 to 2 equivalents) in CH_3CN-HEPES buffer solution. Inset: The linear response curve of absorption intensity of SBPQ at 440 nm depending on Al^{3+} concentration. (b) Changes of absorption spectra of SBPQ (20 μM) upon addition of 2 equivalents of different metal ions.

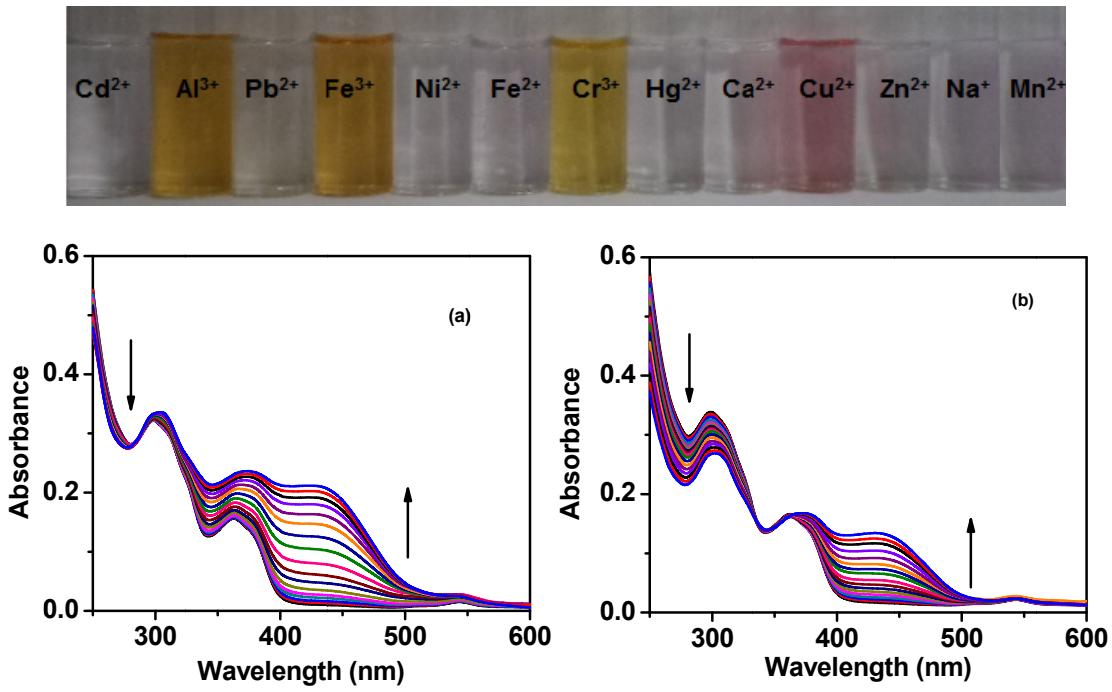

Figure S4: (Up) A photograph showing the colour change of SBPQ (20 μM) after addition of different metal ions stated (2 equivalents). (Below) Change of absorption

spectra of SBPQ (20 μM) upon gradual addition of (a) Fe^{3+} and (b) Cr^{3+} (0 to 2 equivalents) in CH_3CN-HEPES buffer solution.

7. Living cell imaging System

The imaging system was comprised of an inverted fluorescence microscope (Leica DM 1000 LED), digital compact camera (Leica DFC 420C) and an image processor (Leica Application Suite v3.3.0). The microscope was equipped with a mercury 50 watt lamp.

Preparation of Cells for imaging

Candida albicans cells (IMTECH No. 3018) and *Bacillus* sp. (strain isolated in our laboratory as a bio-pesticide agent for controlling looper pest of tea and identified on the basis of 16S rDNA gene sequence homology) cells from exponentially growing culture in potato dextrose broth (pH 5.2, incubation temperature 37 ^{0}C) and Nutrient broth (pH 7.2, incubation temperature 29^{0}C) respectively were collected by centrifugation at 3000 rpm for 05 minutes. Pollen grains were obtained from freshly collected mature buds of *Tecoma stans*, a common ornamental plant of Bignoniaceae family. After crushing the stamens on a sterile petri plate and suspending them in 0.1 M HEPES buffer (pH 7.4), debris were removed by filtering through a thin layer of non absorbent cotton. Suspended pollens were subjected to centrifugation at 3000 rpm for 5 min. All three types of cells were washed twice by suspending them in 0.1 M HEPES buffer (pH 7.4) followed by centrifugation in the same speed as above. Then washed cells were treated separately with 5 μM Aluminium nitrate for 30 minutes. After incubation, the cells were again washed with 0.1 M HEPES buffer (pH 7.4) and then incubated with 5 μM SBPQ for another 30 minutes. Treated cells are washed to reduce background fluorescence and then mounted on grease free glass slide and observed under a Leica DM 1000 Fluorescence microscope with UV filter. Cells treated Aluminium nitrate but not with ligand SBPQ and

cells without Aluminium nitrate treatment but incubated with ligand SBPQ were used as control. We also performed the reverse experiment with *Candida albicans* cells i.e. the cells incubated first with SBPQ, washed and then treated with Aluminium nitrate and observed the fluorescence under the microscope.

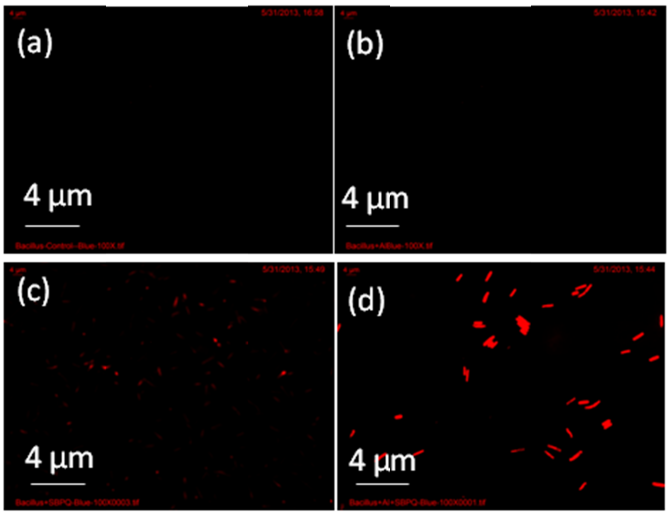

Figure S5: Fluorescence Microscopic photographs of (a) *Bacillus thuringiensis* cells without any treatment, (b) *B. thuringiensis* cells treated with 5 µM Aluminium nitrate, (c) *B. thuringiensis* cells treated with 5 µM SBPQ, (d) *B. thuringiensis* cells treated with 5 µM aluminium nitrate, washed and then treated with 5 µM SBPQ.

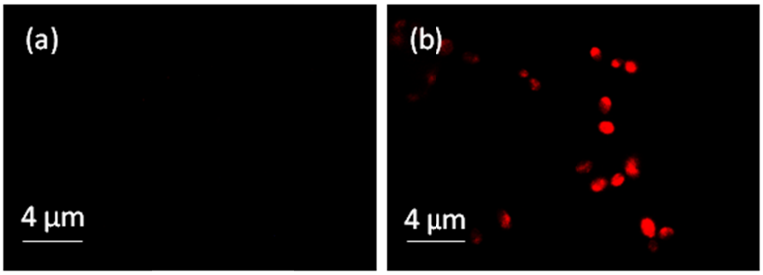

Figure S6: Fluorescence Microscopic photographs of (a) *Candida albicans* cells treated with 5 µM SBPQ, (b) *C. albicans* cells treated with 5 µM SBPQ, washed and then treated with 5 µM aluminium nitrate.

8. Determination of fluorescence Quantum Yields (Φ) of SBPQ and its complex with trivalent ions:

For measurement of the quantum yields of SBPQ and its complex (in situ, after addition of 1 equivalent of each metal ion) with Al^{3+}, Fe^{3+} and Cr^{3+}, we recorded the absorbance of the compounds in acetonitrile solution. The emission spectra were recorded using the maximal excitation wavelengths, and the integrated areas of the fluorescence-corrected spectra were measured. The quantum yields were then calculated by comparison with rhodamine B (Φs = 0.66 in ethanol) as reference using the following equation:

$$\Phi x = \Phi s \times \left(\frac{Ix}{Is}\right) \times \left(\frac{As}{Ax}\right) \times \left(\frac{nx}{ns}\right)^2$$

Where, x & s indicate the unknown and standard solution respectively, Φ is the quantum yield, *I* is the integrated area under the fluorescence spectra, *A* is the absorbance and *n* is the refractive index of the solvent.

We calculated the quantum yields of SBPQ and SBPQ-Al^{3+}, SBPQ-Cr^{3+} and SBPQ-Fe^{3+} using the above equation and the values are 0.01, 0.42, 0.18 and 0.25 respectively.

9. General procedure for drawing Job's plot by fluorescence method:

Stock solution of same concentration of sensor and M^{3+} (where M = Fe^{3+}, Al^{3+} and Cr^{3+}) were prepared in the order of 20 μM in [CH_3CN/ H_2O, 1/1, v/v] (at 25 °C) at pH 7.4 in HEPES buffer. The emission spectrum in each case with different *host–guest* ratio but equal in volume was recorded. Job's plots were drawn by plotting $\Delta I.X_{host}$ *vs* X_{host} (ΔI = change of intensity of the emission spectrum at 675 nm during titration and X_{host} is the mole fraction of the host in each case, respectively).

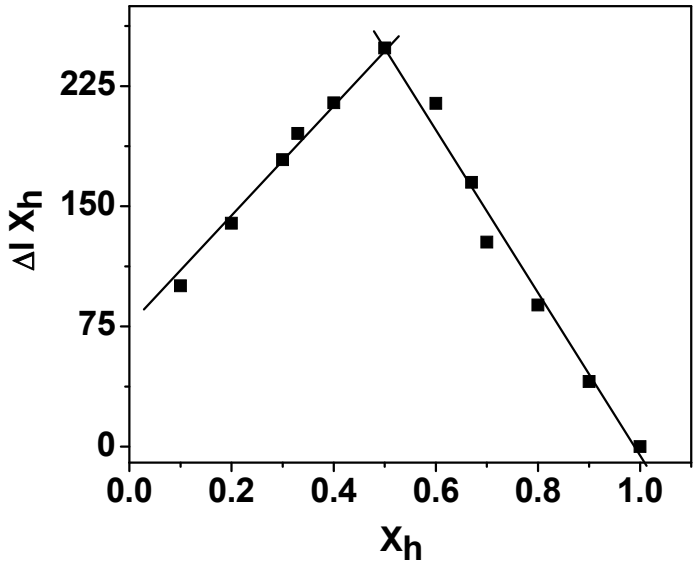

Figure S7: Job's plot diagram of receptor for Al^{3+} (where X_h is the mole fraction of the host and ΔI indicates the change of emission intensity at 675 nm)

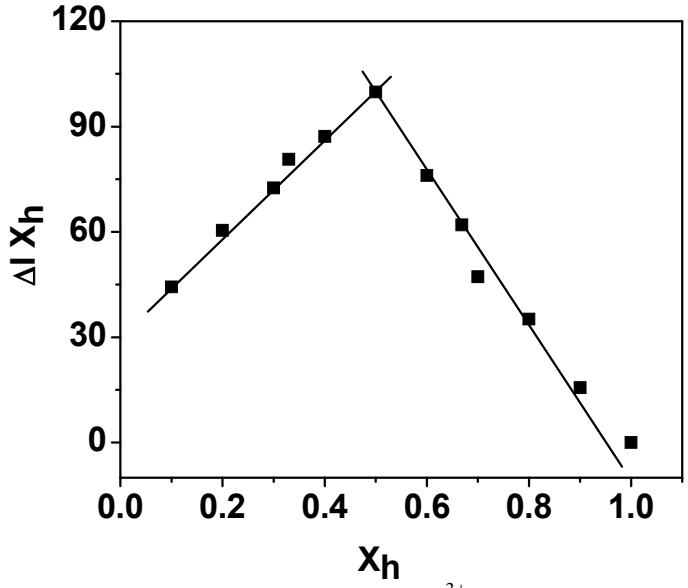

Figure S8: Job's plot diagram of receptor for Fe^{3+} (where X_h is the mole fraction of the host and ΔI indicates the change of emission intensity at 675 nm)

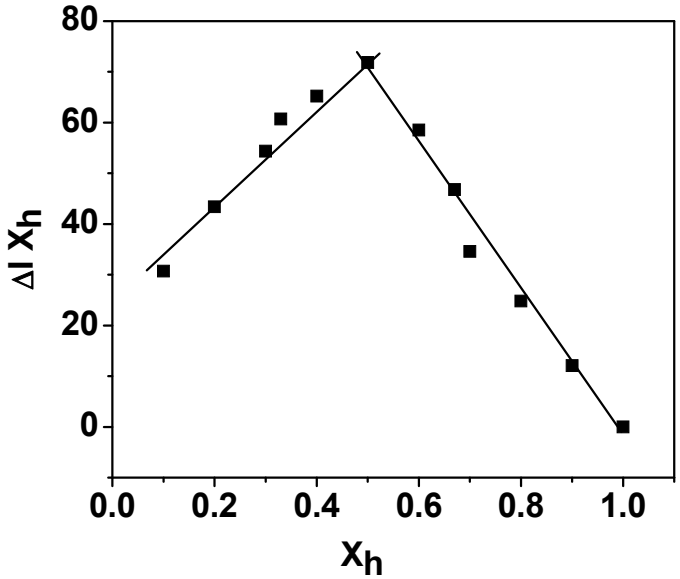

Figure S9: Job's plot diagram of receptor for Cr^{3+} (where X_h is the mole fraction of the host and ΔI indicates the change of emission intensity at 675 nm)

10. Determination of detection limit:

The detection limit was calculated based on the fluorescence titration. To determine the S/N ratio, the emission intensity of SBPQ without trivalent ions (Al^{3+}, Fe^{3+} and Cr^{3+}) was measured by 10 times and the standard deviation of blank measurements was determined. The detection limit (DL) of **SBPQ** for Al^{3+}, Fe^{3+} and Cr^{3+} were determined from the following equation[1]:

$DL = K \times Sb_1/S$

Where K = 2 or 3 (we take 3 in this case); Sb_1 is the standard deviation of the blank solution; S is the slope of the calibration curve.

For Al^{3+}:

From the graph we get slope = 5.05×10^7, and Sb_1 value is 0.54644

Thus using the formula we get the Detection Limit = 3.24×10^{-8} M i.e. SBPQ can detect Al^{3+} in this minimum concentration by fluorescence techniques.

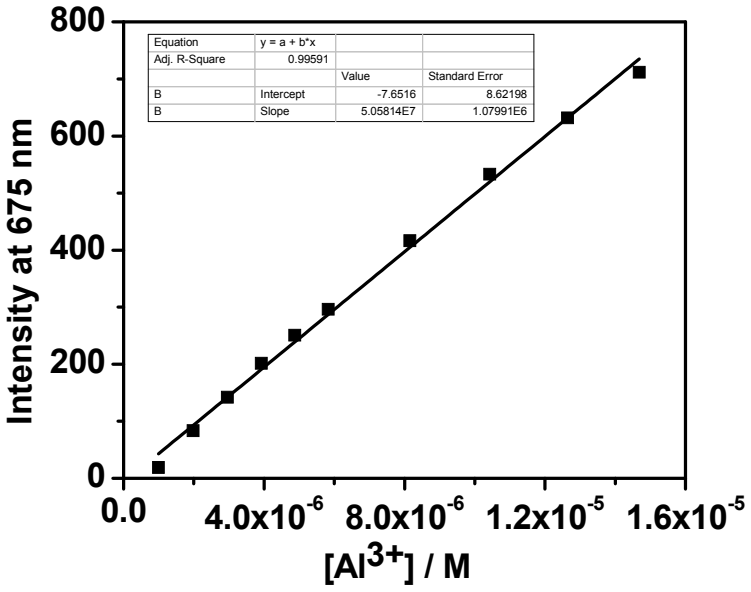

Figure S10: Linear response curve of SBPQ at 675 nm depending on the Al^{3+} concentration.

For Fe^{3+}:

From the graph we get slope = 1.882×10^{7}, and Sb_1 value is 0.56794

Thus using the formula we get the Detection Limit = 9.05×10^{-8} M i.e. SBPQ can detect Fe^{3+} in this minimum concentration.

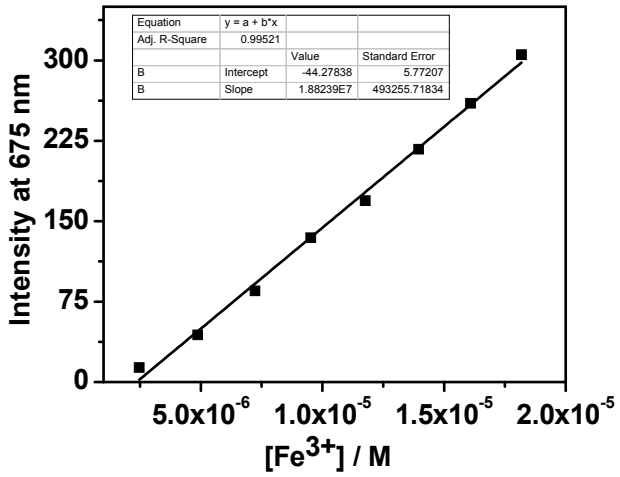

Figure S11: Linear response curve of SBPQ at 675 nm depending on the Fe^{3+} concentration.

For Cr^{3+}:

From the graph we get slope = 1.76×10^{7}, and Sb_1 value is 0.54784

Thus using the formula we get the Detection Limit = 9.33×10^{-8} M i.e. SBPQ can detect Cr^{3+} in this minimum concentration.

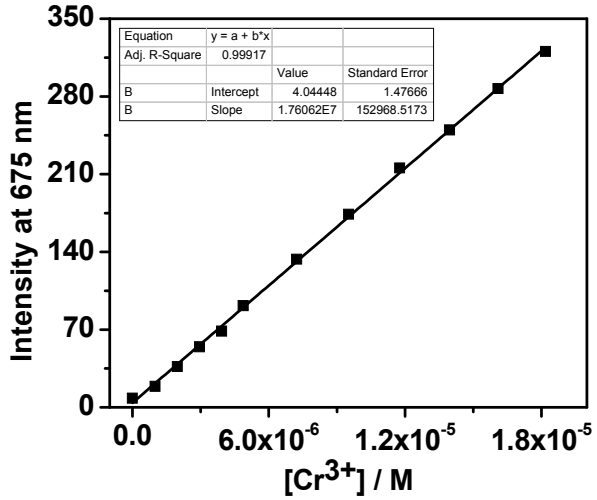

Figure S12: Linear response curve of SBPQ at 675 nm depending on the Cr^{3+} concentration.

11. Metal ion selectivity profile of the sensor :

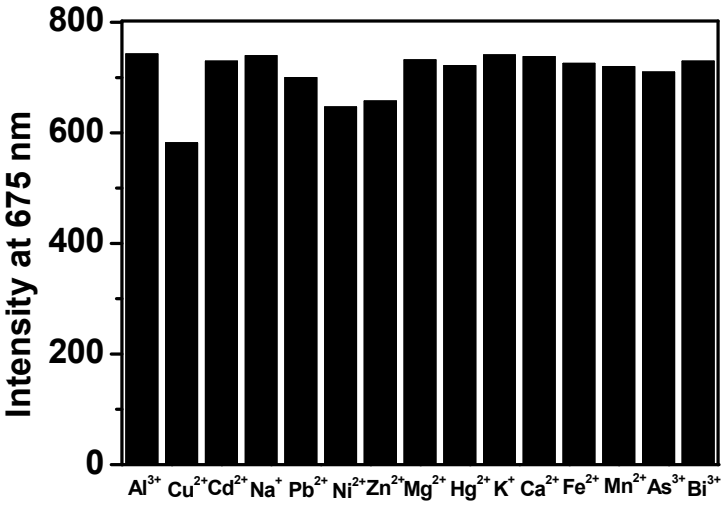

Figure S13: Change in emission intensity of SBPQ (20 μM) at 675 nm upon addition of 1 equivalents of Al^{3+} along with 2 equivalents of various metal ions. λ_{ex} = 460 nm.

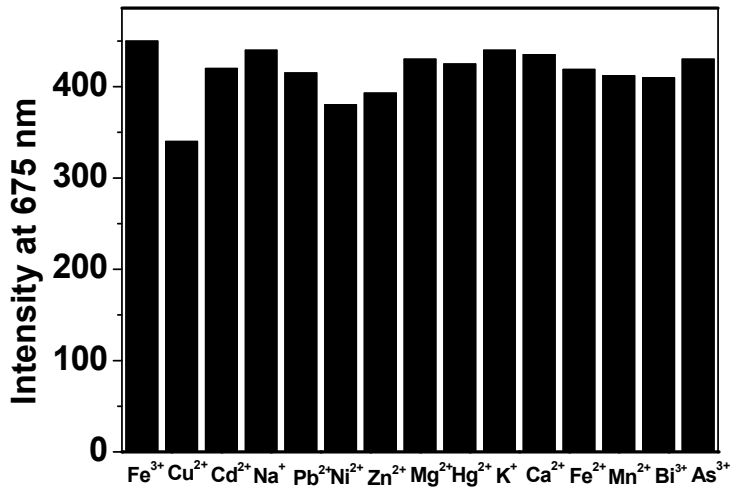

Figure S14: Change in emission intensity of SBPQ (20 μM) at 675 nm upon addition of 1 equivalents Fe^{3+} along with 2 equivalents of various metal ions. λ_{ex} = 460 nm.

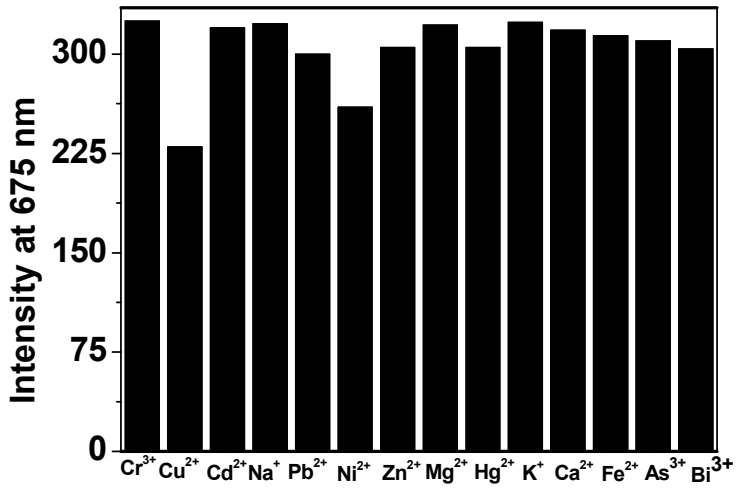

Figure S15: Change in emission intensity of SBPQ (20 μM) at 675 nm upon addition of 1 equivalents Cr^{3+} along with 2 equivalents of various metal ions. λ_{ex} = 460 nm.

12. Computational method:

Full geometry optimizations were carried out using the density functional theory (DFT) method at the B3LYP[2-4] level for the ligand SBPQ in both spiro and ring opening forms and its octahedral Al^{3+} complex. The 6-31+G(d,p) basis set was assigned for the elements. The vibrational frequency calculations were performed to ensure that the optimized geometries represent the local minima and there were only positive eigen values. Vertical electronic excitations based on B3LYP optimized geometries were computed using the time-dependent density functional theory (TDDFT) formalism[5-7] in acetonitrile using conductor-like polarizable continuum model (CPCM)[8-10]. All calculations were performed with Gaussian03 program[11] package with the aid of the GaussView visualization program.

Table S1: Vertical electronic excitations of SBPQ calculated by TDDFT/CPCM method

Excited state	Excitation energy (eV)	λ (nm)	Osc. Strength (f)	Key transitions
1	3.1213	397.2	0.0473	(98%)HOMO → LUMO
2	3.3596	369.1	0.1727	(95%)HOMO-1 → LUMO
7	3.8131	325.2	0.4030	(80%)HOMO-3 → LUMO
21	4.6247	268.1	0.3208	(77%)HOMO-4 → LUMO+2

Table S2: Vertical electronic excitations of SBPQ in ring opened form calculated by TDDFT/CPCM method

Excited state	Excitation energy(eV)	λ (nm)	Osc. Strength (f)	Key transitions
1	2.2923	540.9	0.9060	(97%)HOMO → LUMO
3	2.9487	420.5	0.0760	(72%)HOMO → LUMO+1
4	3.1184	397.6	0.3797	(79%)HOMO-1 → LUMO
8	3.7409	331.4	0.2154	(82%)HOMO-1 → LUMO+1
26	4.5232	274.1	0.2630	(71%)HOMO-10 → LUMO

Table S3: Vertical electronic excitations of Al^{3+} complex of SBPQ calculated by TDDFT/CPCM method

Excited state	Excitation energy (eV)	λ (nm)	Osc. Strength (f)	Key transitions
1	2.2417	553.1	0.0659	(98%)HOMO → LUMO
3	2.7355	453.2	0.6167	(90%)HOMO → LUMO+2
4	2.8960	428.1	0.3926	(86%)HOMO-1 → LUMO
6	3.3357	371.7	0.1423	(69%)HOMO → LUMO+3
8	3.4466	359.7	0.1168	(67%)HOMO-2 → LUMO

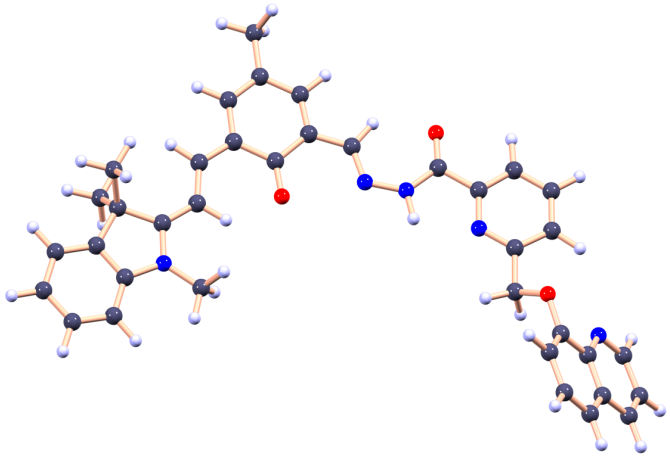

Figure S16: Optimized structure of SBPQ ring opening form calculated by DFT/B3LYP/6-31+G(d,p) method

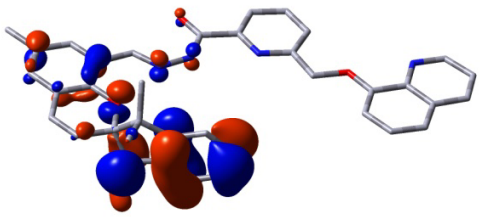	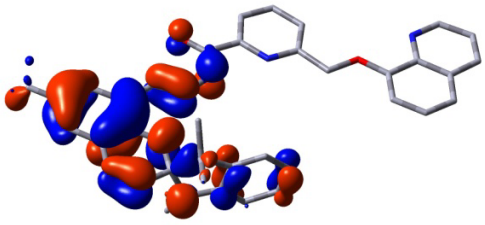
HOMO (E = -5.14 eV)	HOMO-1 (E = -5.42 eV)
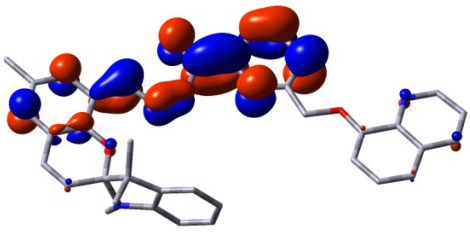	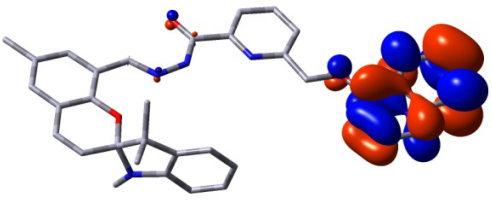
LUMO (E = -1.54 eV)	LUMO+1 (E = -1.34 eV)

Figure S17: Contour plot of some selected molecular orbitals of SBPQ

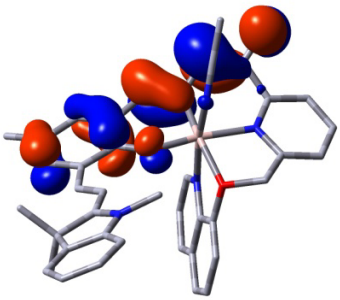	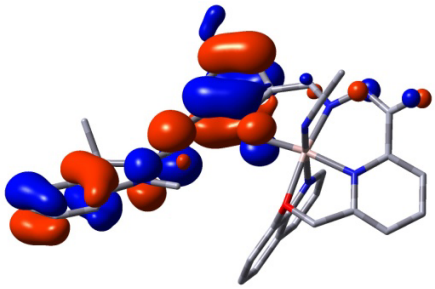
HOMO (E = -9.90 eV)	HOMO-1 (E = -10.59 eV)
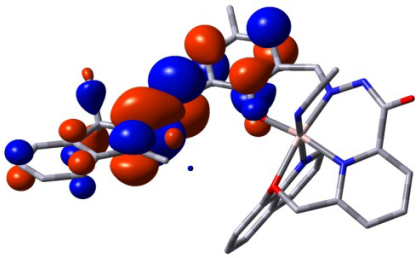	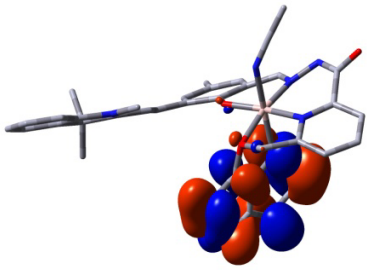
LUMO (E = -7.55 eV)	LUMO+1 (E = -7.45 eV)

Figure S18: Contour plot of some selected molecular orbitals of Al^{3+} complex of SBPQ

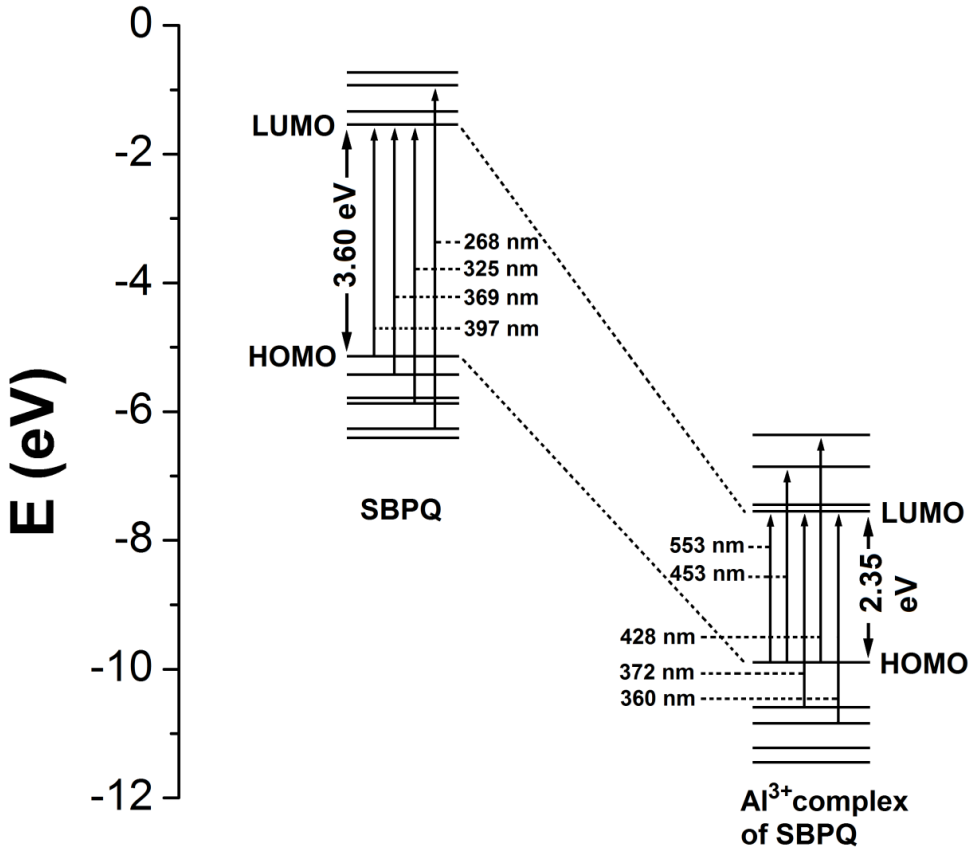

Figure S19: Energy level co-relational diagram of molecular orbitals and some selected calculated electronic transitions of SBPQ and its Al^{3+} complex.

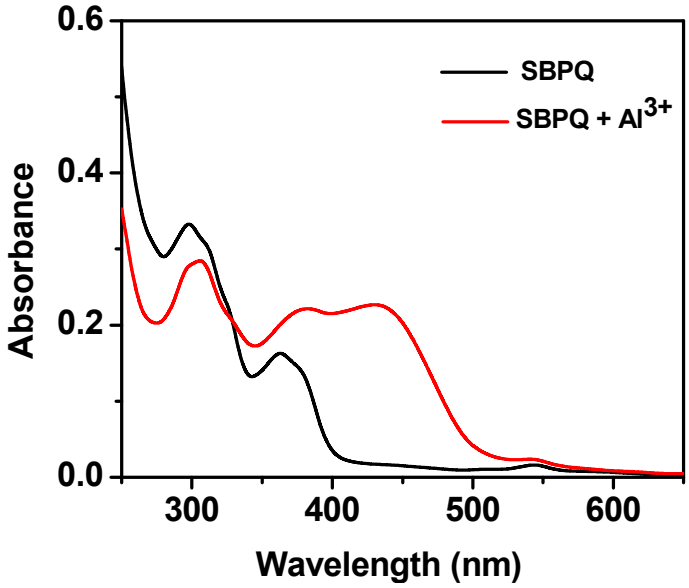

Figure S20: Experimental electronic spectra of SBPQ and its Al^{3+} complex

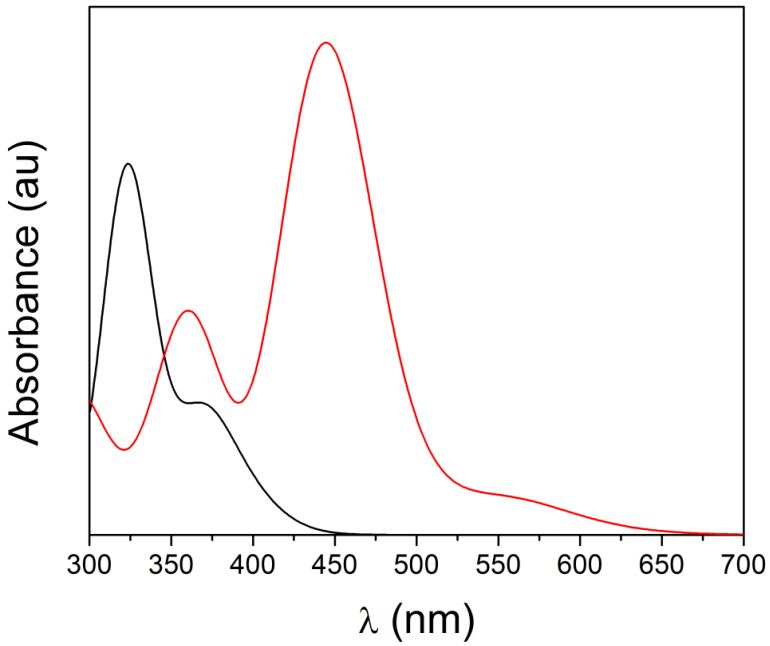

Figure S21: Calculated electronic spectra of SBPQ (—) and its Al^{3+} complex (—) by TDDFT method

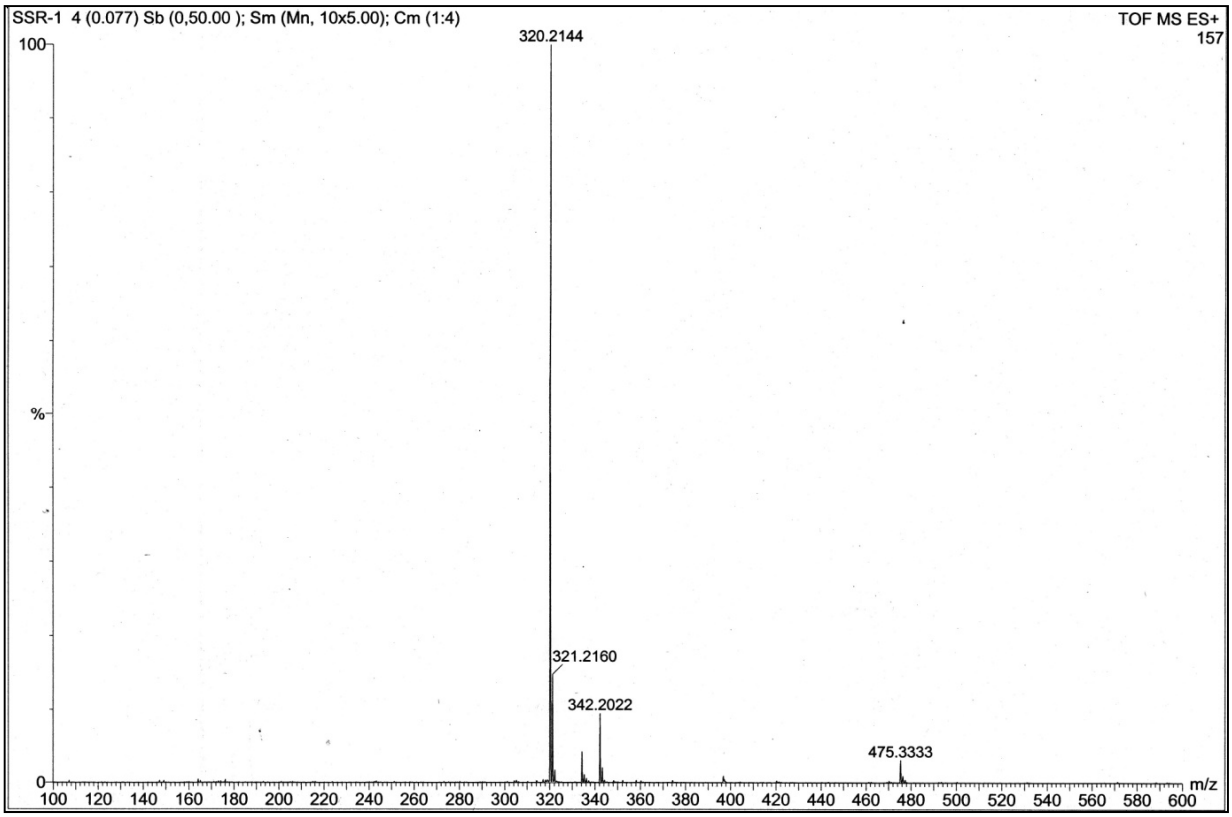

Figure S22: HRMS spectrum of R1

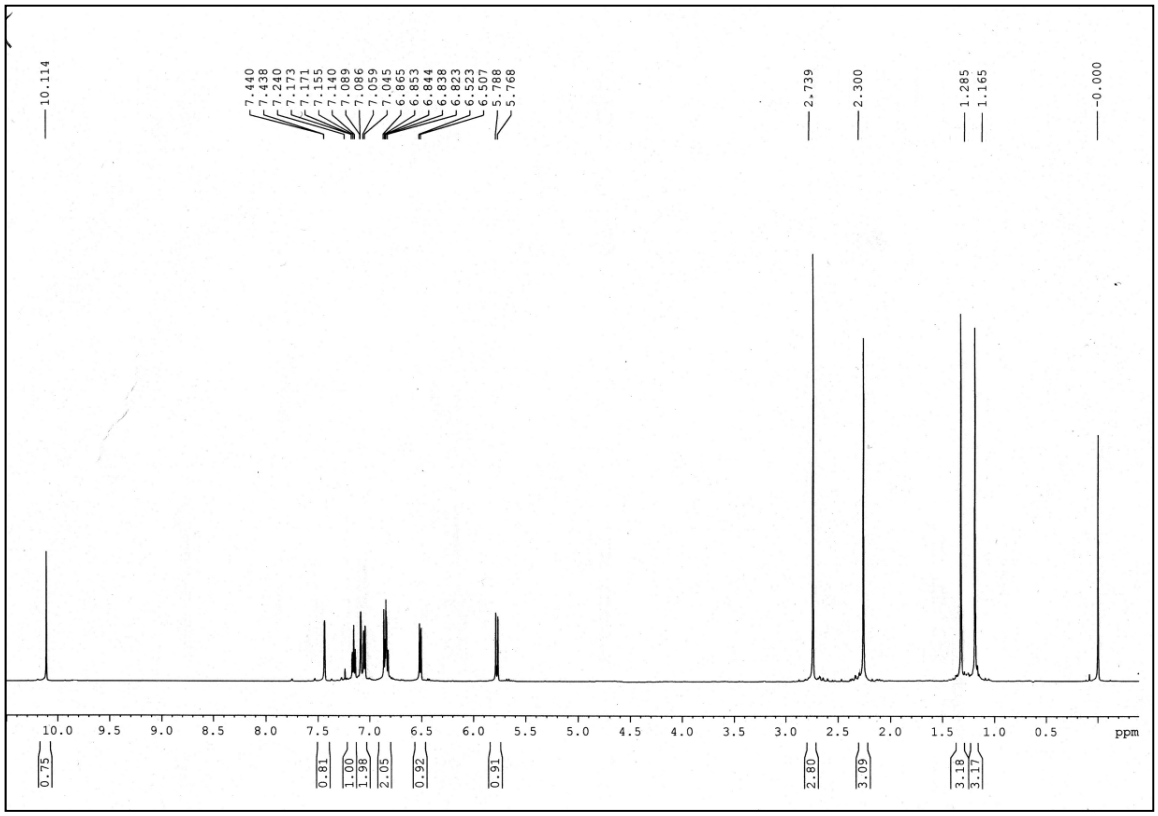

Figure S23: ^{1}H NMR (400 MHz) spectrum of R1 in $CDCl_3$.

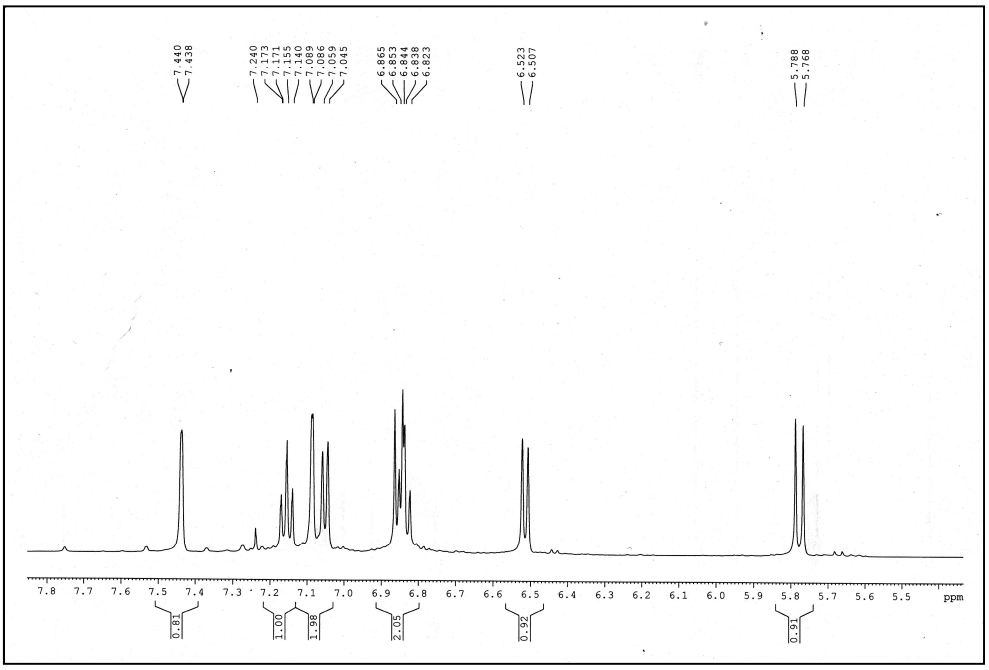

Figure S23a: Expansion mode of ^{1}H NMR (400 MHz) spectrum of R1 in $CDCl_3$.

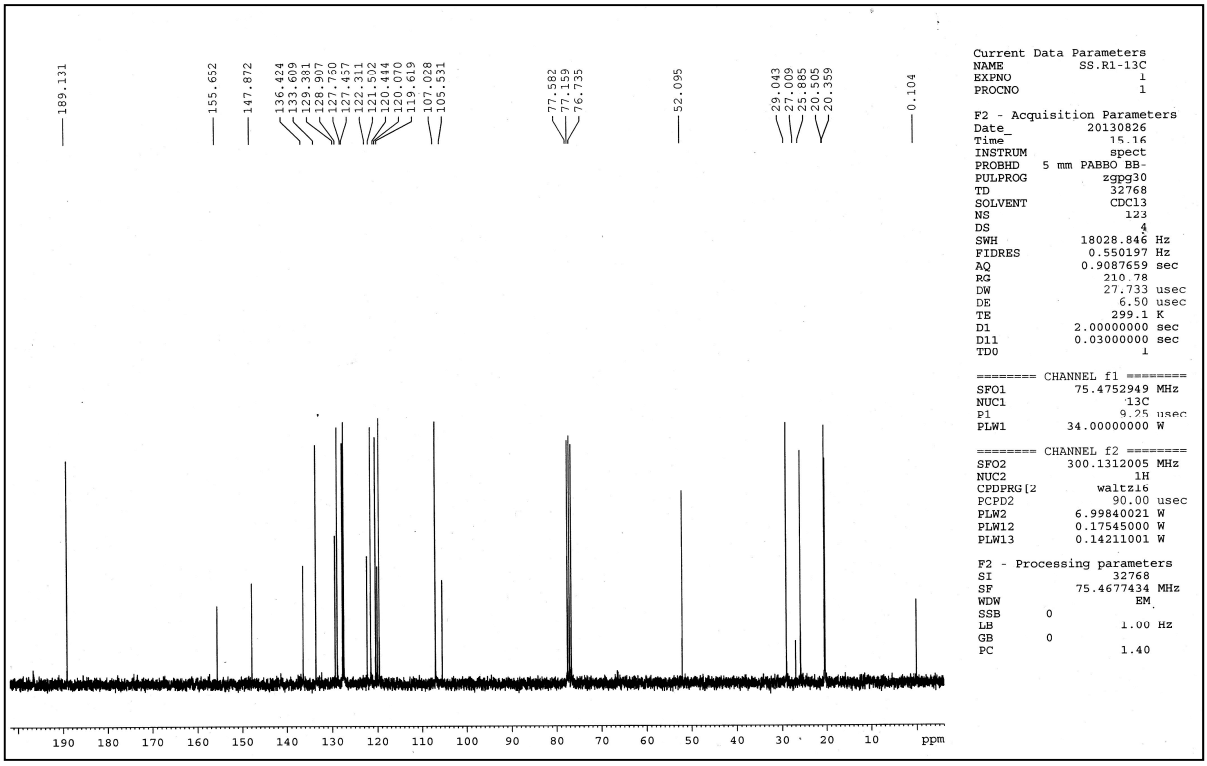

Figure S24: ^{13}C NMR (75 MHz) spectrum of R1 in $CDCl_3$.

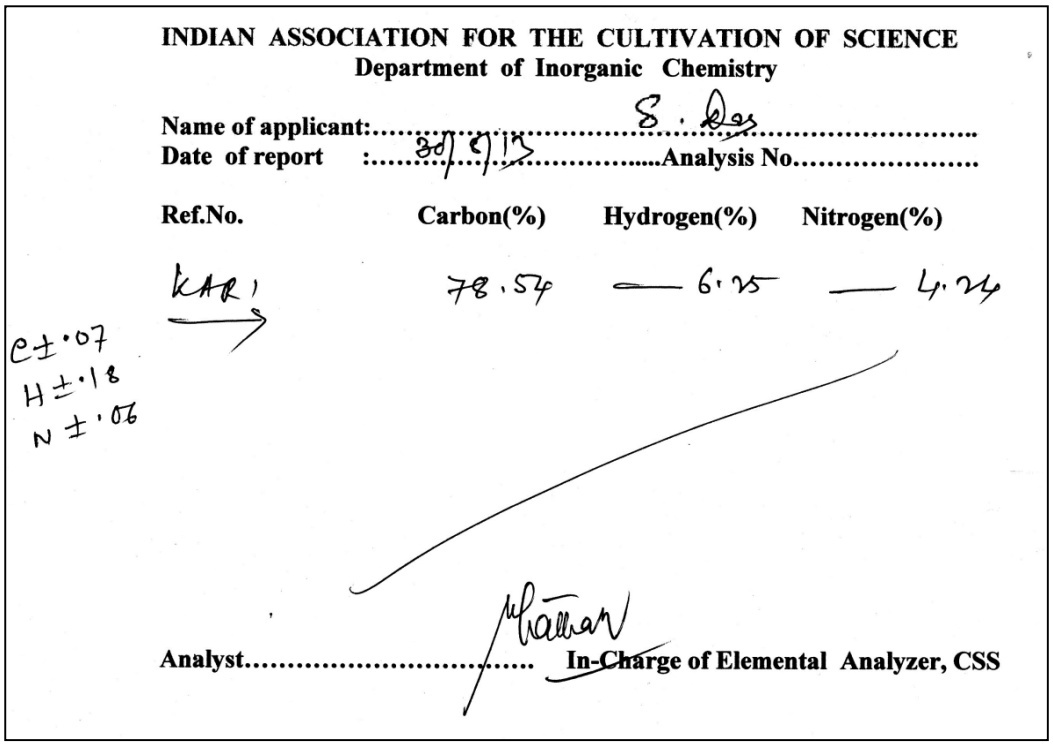

Figure S25: Scan copy of elemental analysis of R1

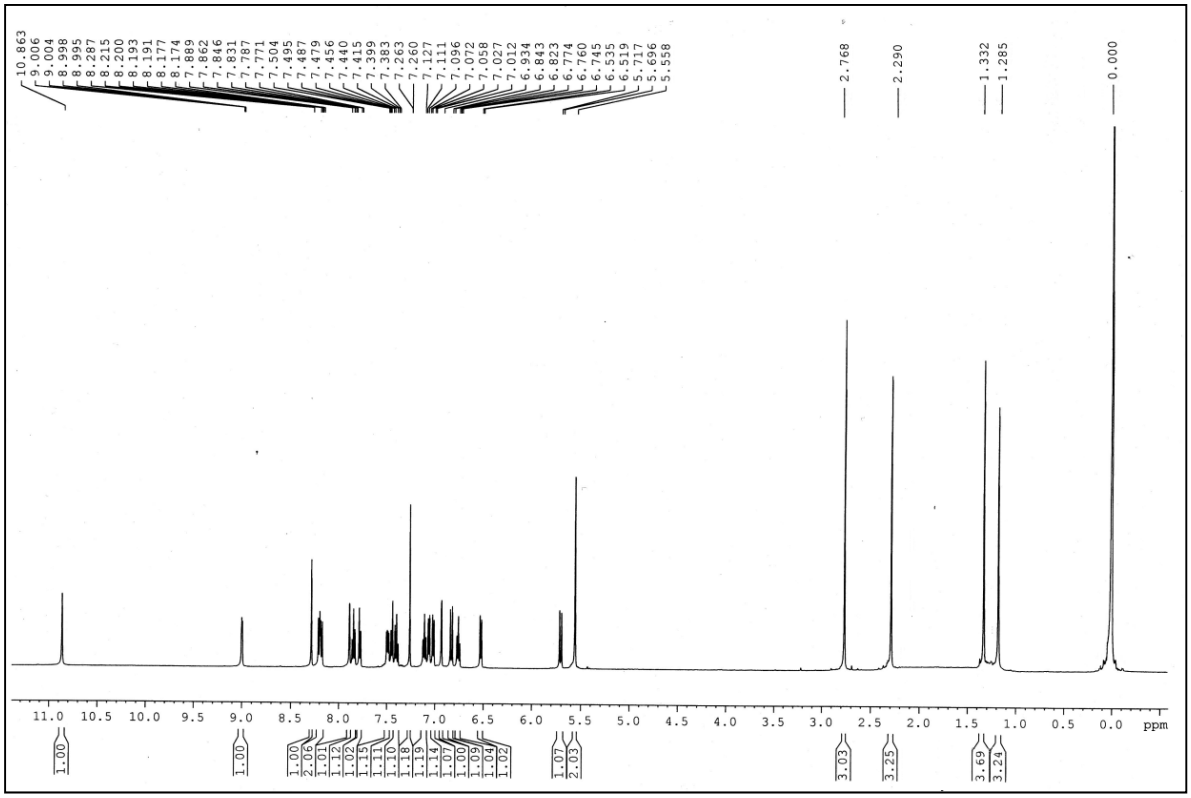

S26: ^{1}H NMR (400 MHz) spectrum of SBPQ in $CDCl_3$.

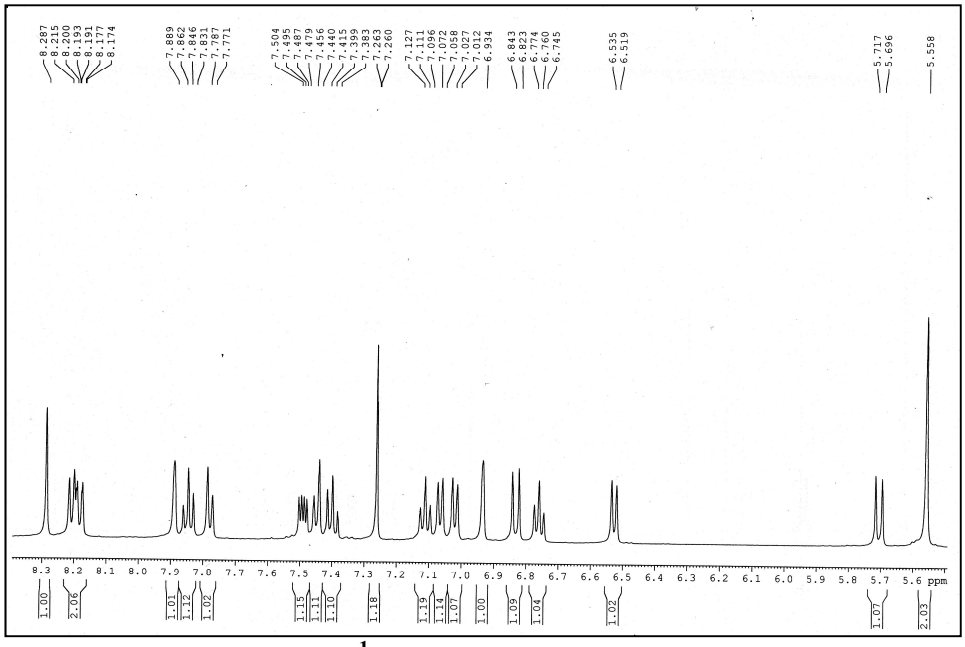

S26a: Partial expansion of ^{1}H NMR (400 MHz) spectrum of SBPQ in $CDCl_3$.

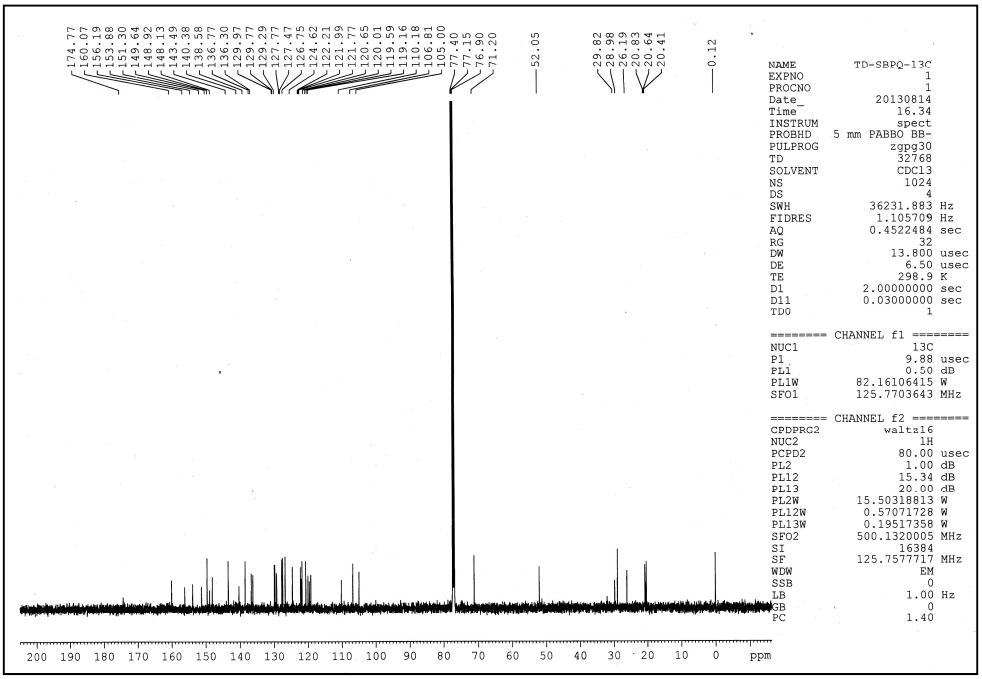

Figure S27: ^{13}C NMR (125 MHz) spectrum of SBPQ in $CDCl_3$.

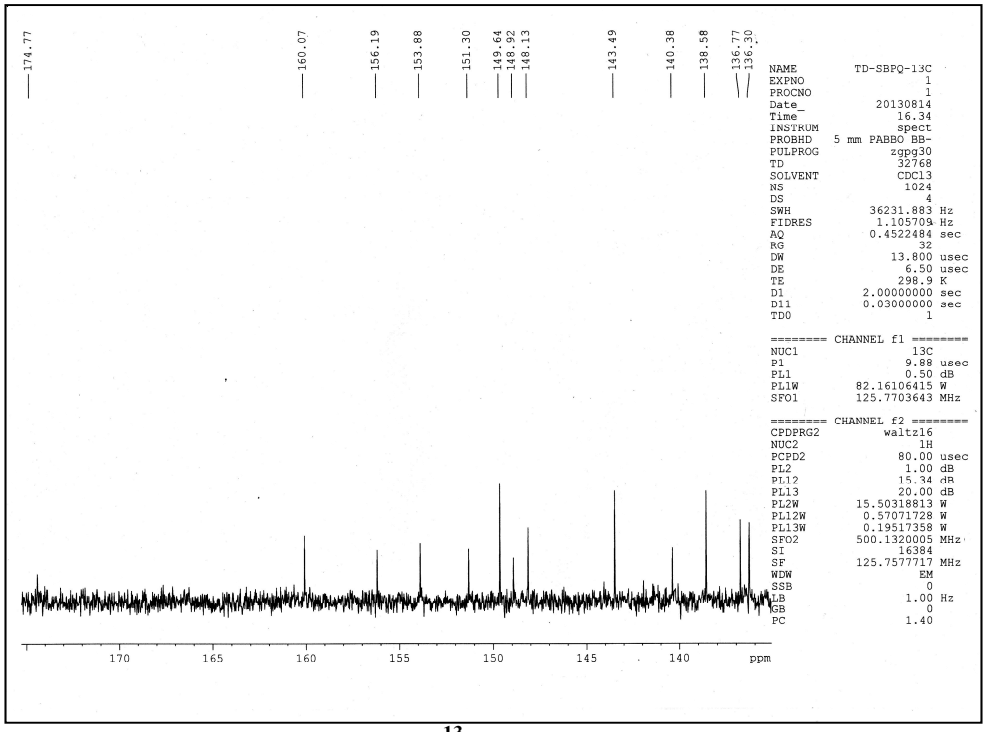

Figure S27a: Expansion mode of ^{13}C NMR (125 MHz) spectrum of SBPQ in $CDCl_3$.

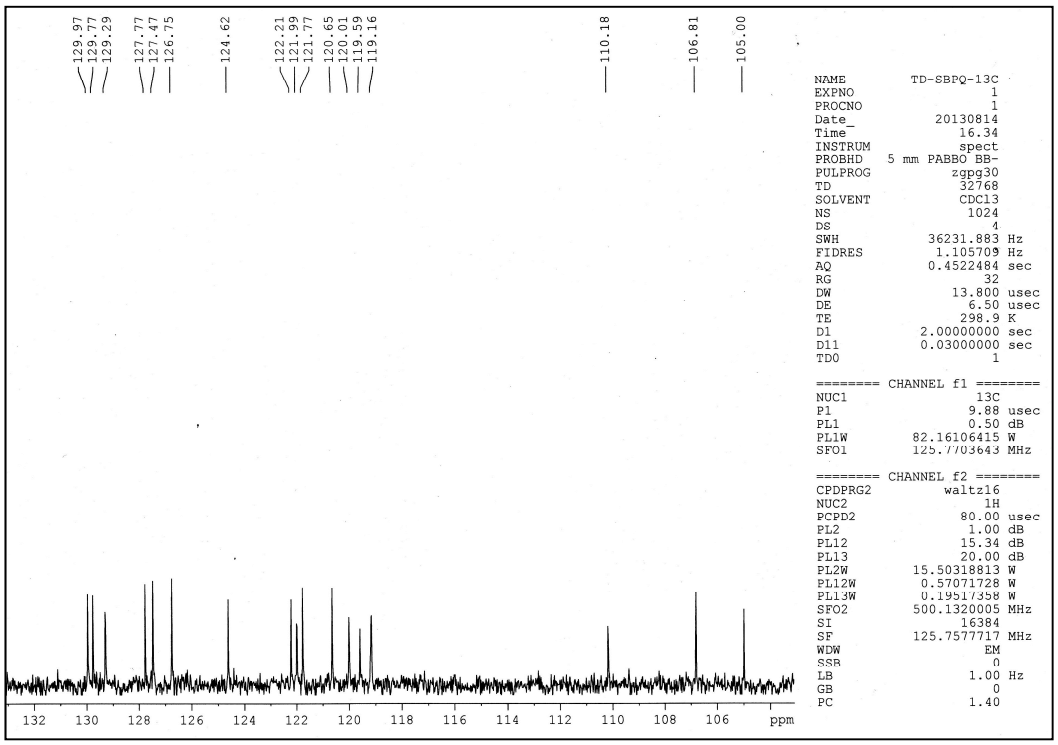

Figure S27b: Expansion mode of ^{13}C NMR (125 MHz) spectrum of SBPQ in $CDCl_3$.

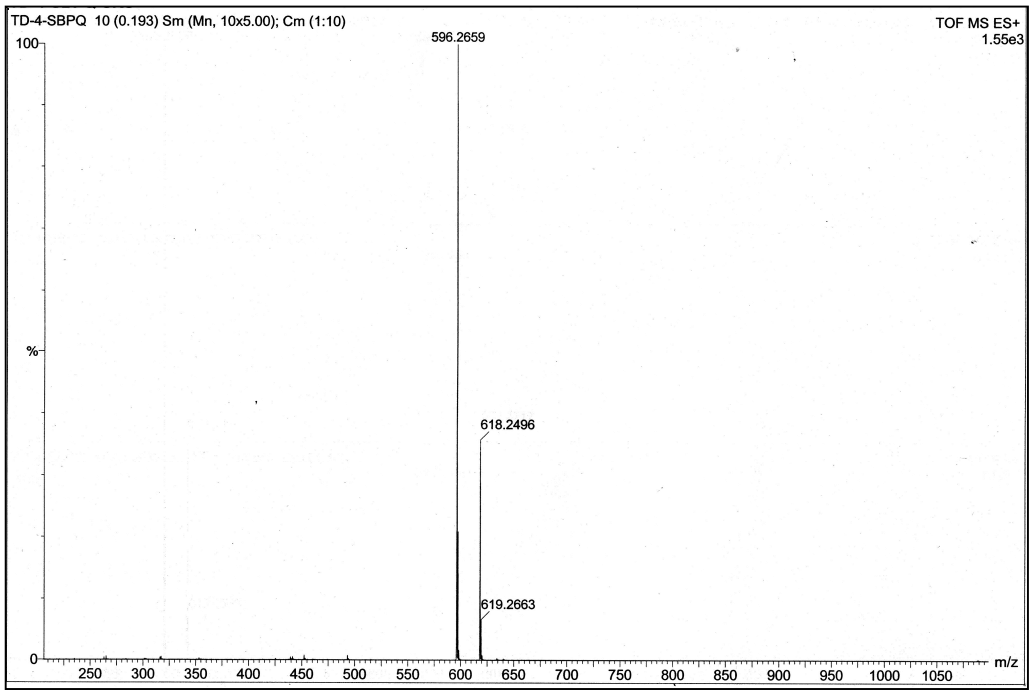

Figure S28: HRMS spectrum of SBPQ.

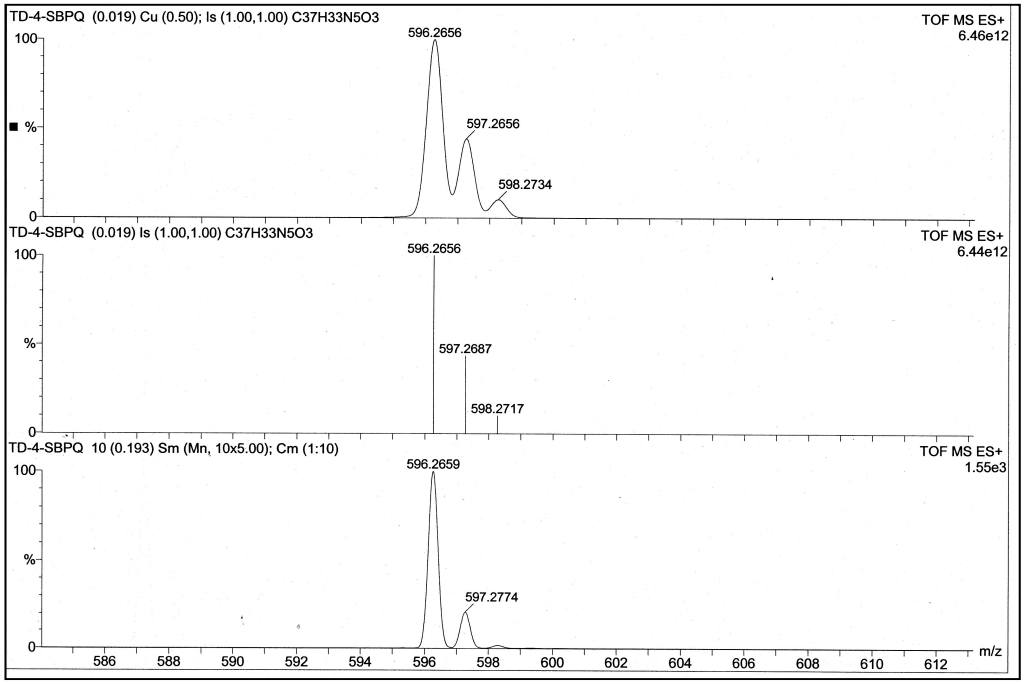

Figure S28a: Expansion of HRMS spectrum of SBPQ.

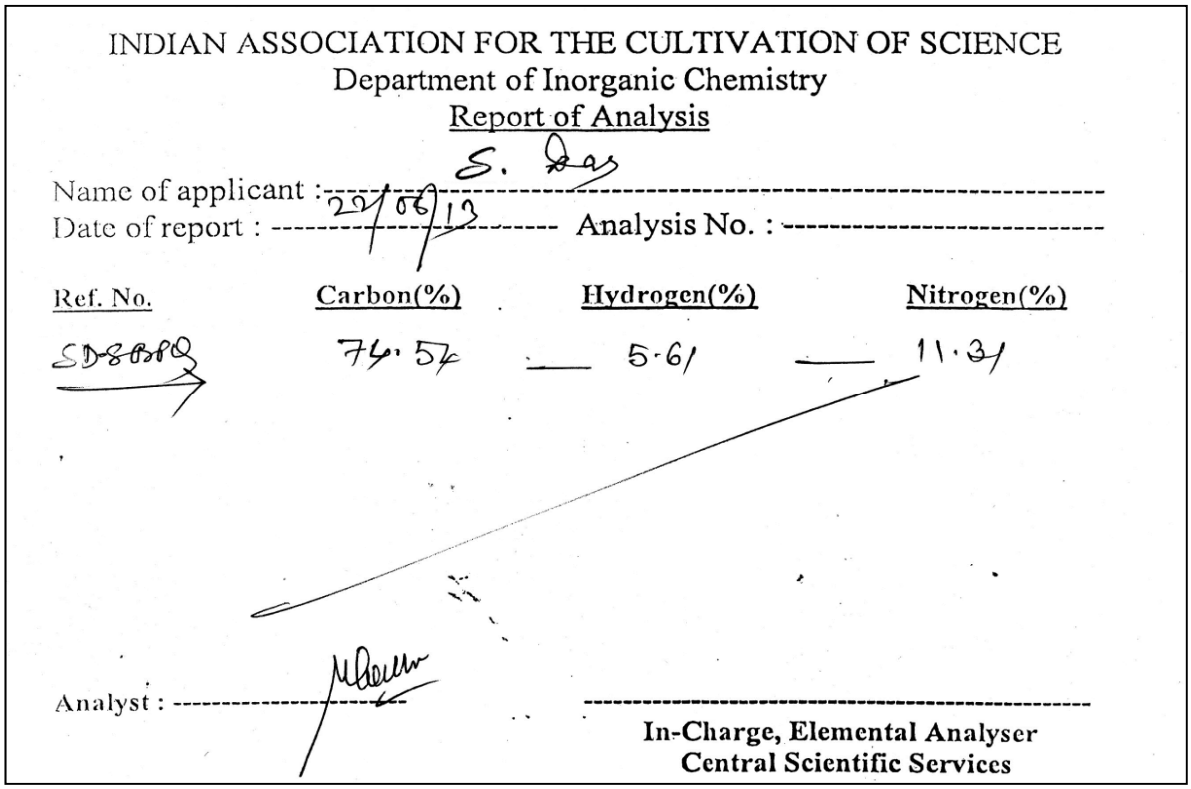

INDIAN ASSOCIATION FOR THE CULTIVATION OF SCIENCE
Department of Inorganic Chemistry
Report of Analysis

Name of applicant : S. Das
Date of report : 29/06/13 Analysis No. :

Ref. No.	Carbon(%)	Hydrogen(%)	Nitrogen(%)
SDBBPQ	74.57	5.61	11.31

Analyst :

In-Charge, Elemental Analyser
Central Scientific Services

Figure S29: Scan copy of elemental analysis of SBPQ

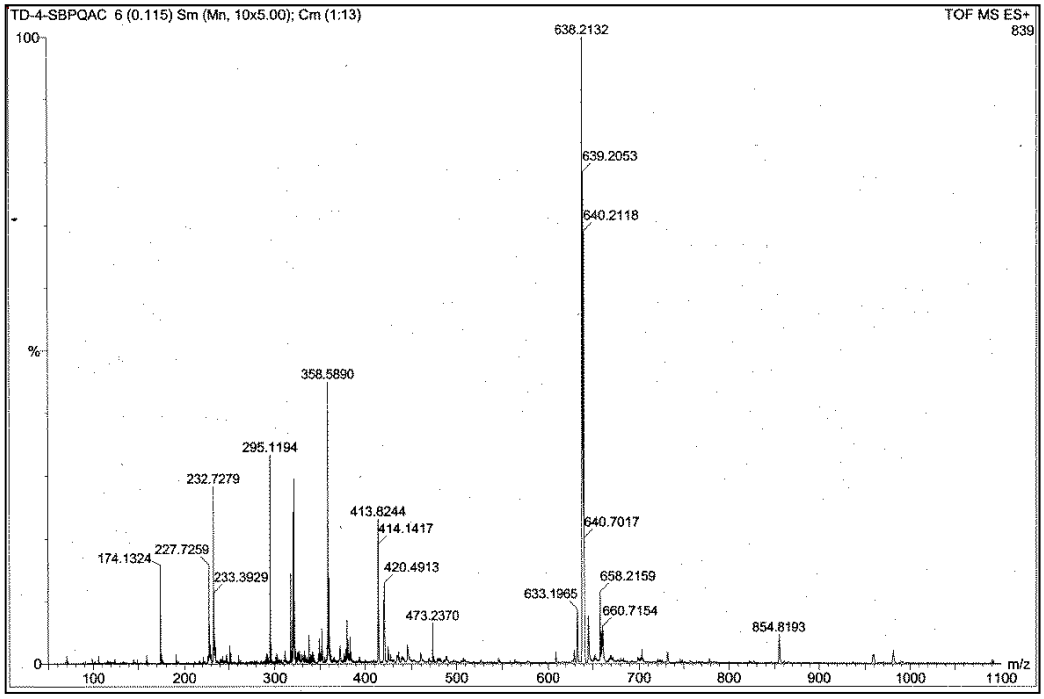

Figure S30: HRMS spectrum of SBPQ-Al complex.

Figure S31: FT-IR spectra of SBPQ and SBPQ-Al complex.

13. Fluorescence titration spectra of receptor with different guest cations:

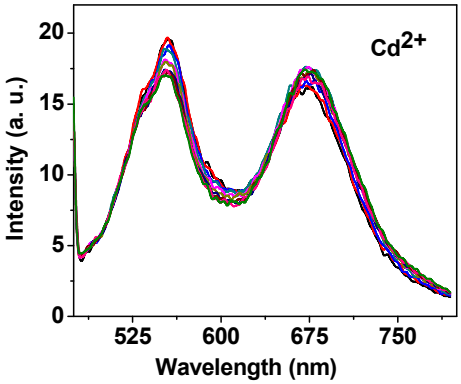

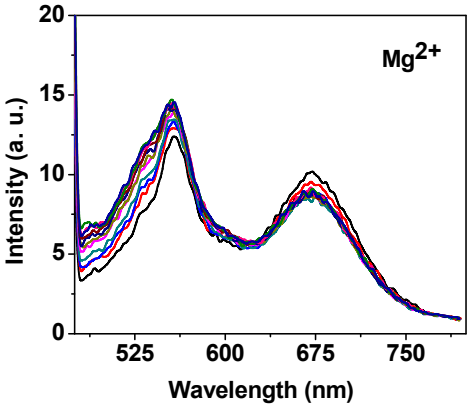

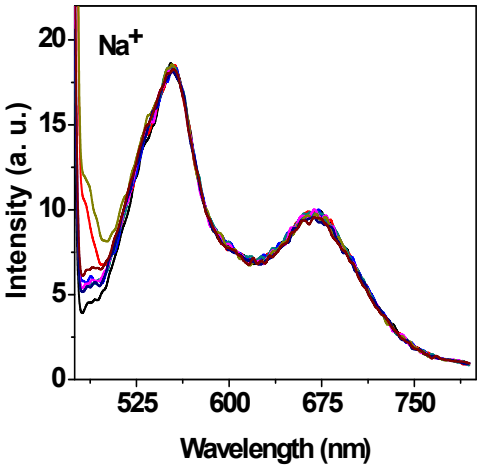

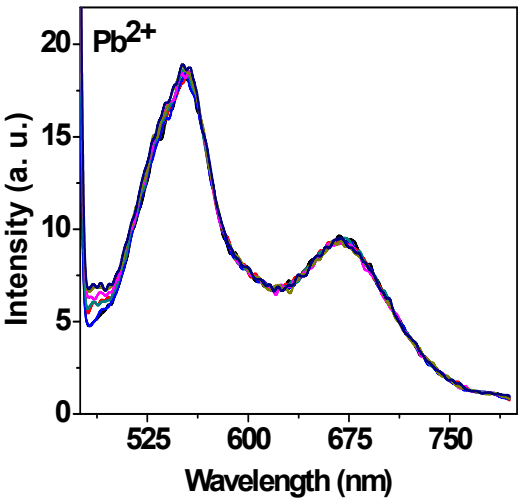

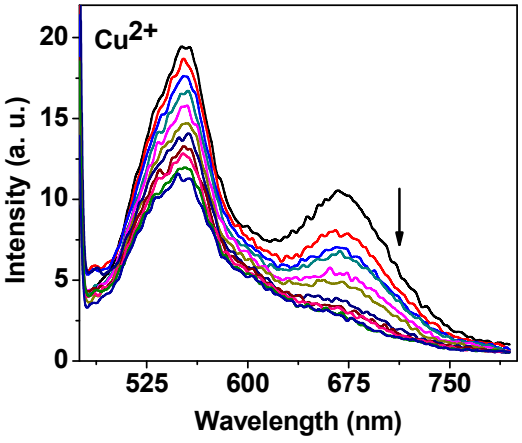

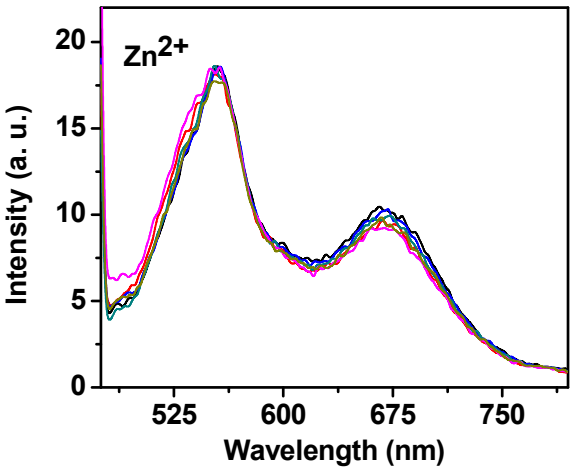

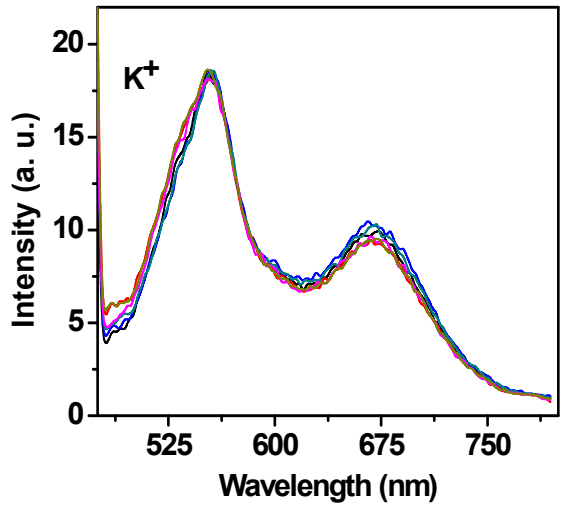
K+
Intensity (a. u.)
Wavelength (nm)
0
5
10
15
20
525
600
675
750

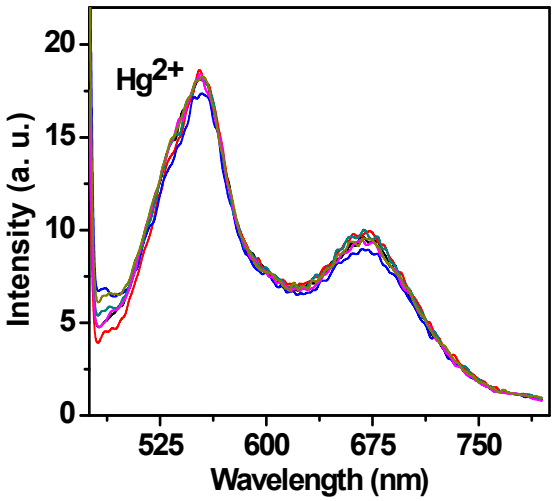
Hg2+
Intensity (a. u.)
Wavelength (nm)
0
5
10
15
20
525
600
675
750

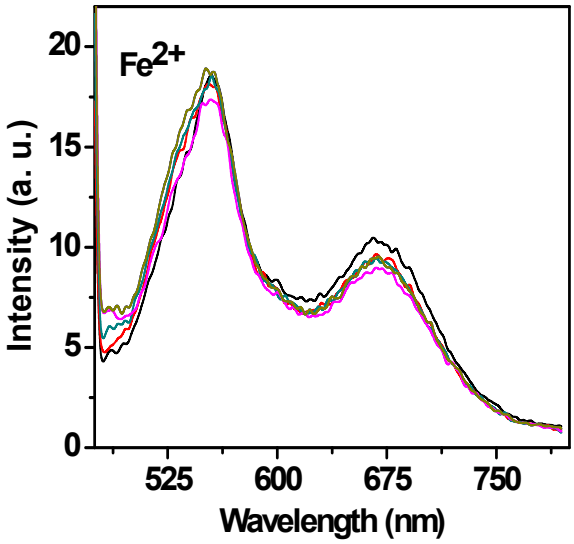
Fe2+
Intensity (a. u.)
Wavelength (nm)
0
5
10
15
20
525
600
675
750

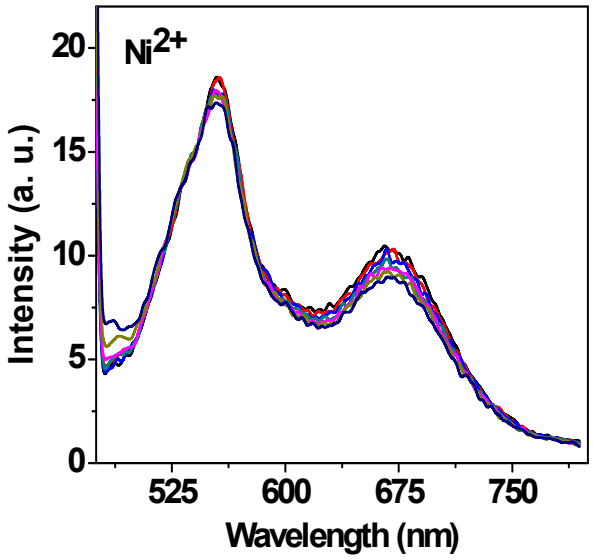
Ni2+
Intensity (a. u.)
Wavelength (nm)
0
5
10
15
20
525
600
675
750

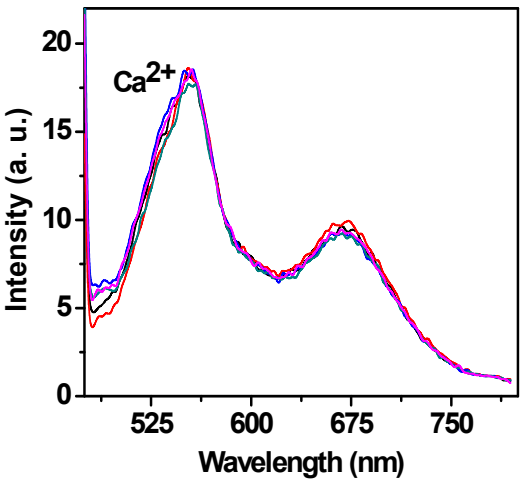
Ca2+
Intensity (a. u.)
Wavelength (nm)
0
5
10
15
20
525
600
675
750

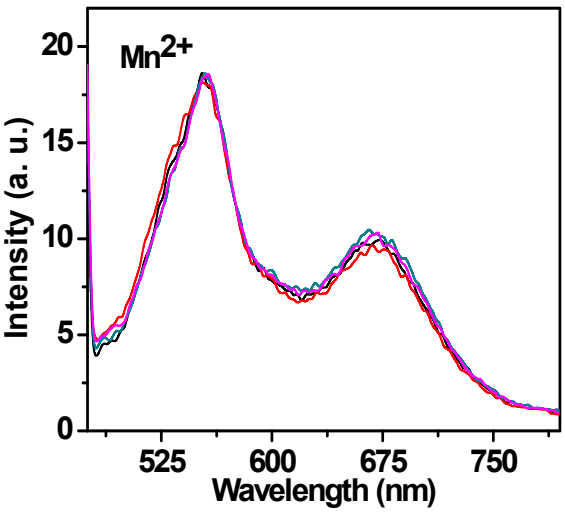
Mn2+
Intensity (a. u.)
Wavelength (nm)
0
5
10
15
20
525
600
675
750

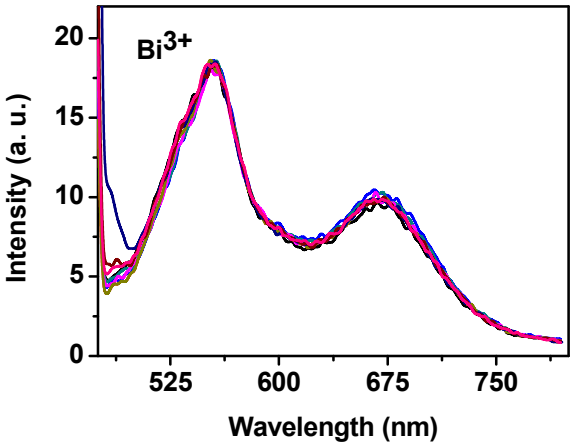

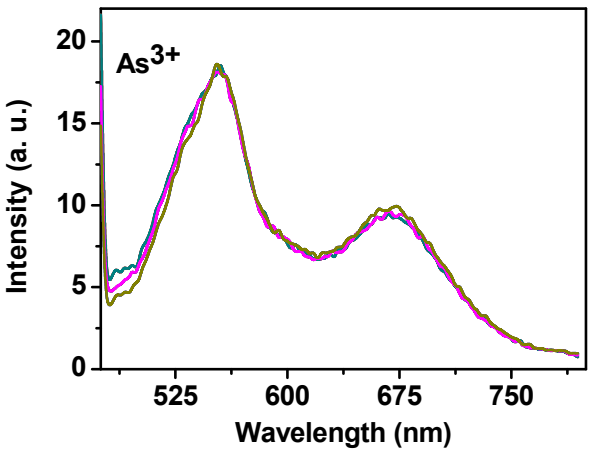

14. UV-vis titration spectra of the sensor with different metal ions:

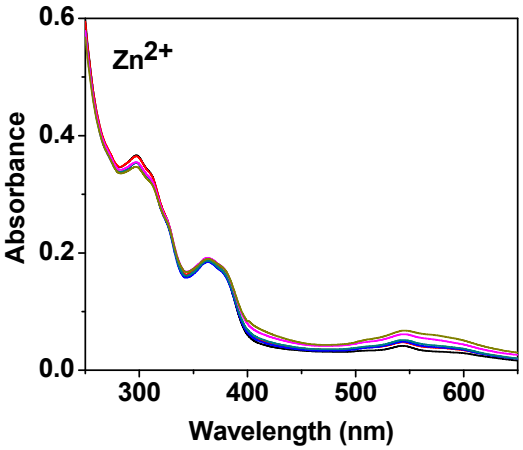

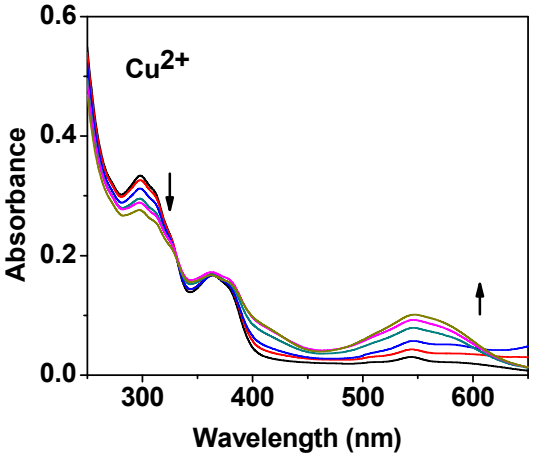

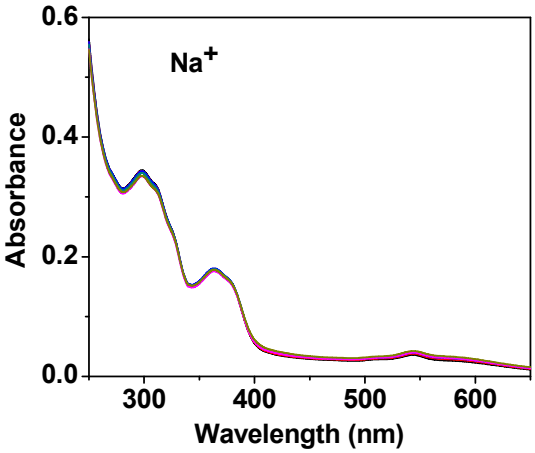

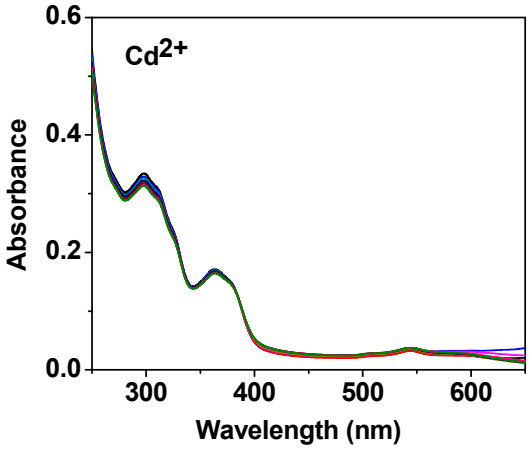

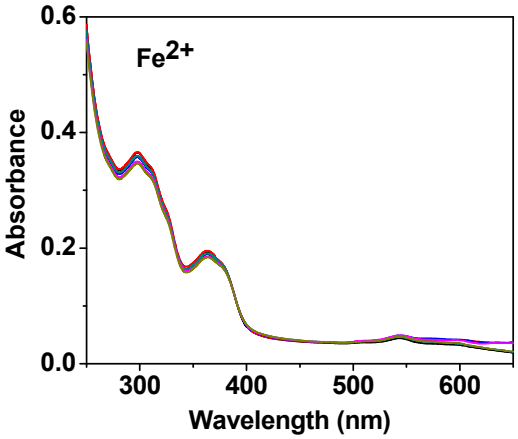
Fe2+
Absorbance
Wavelength (nm)
0.0
0.2
0.4
0.6
300
400
500
600

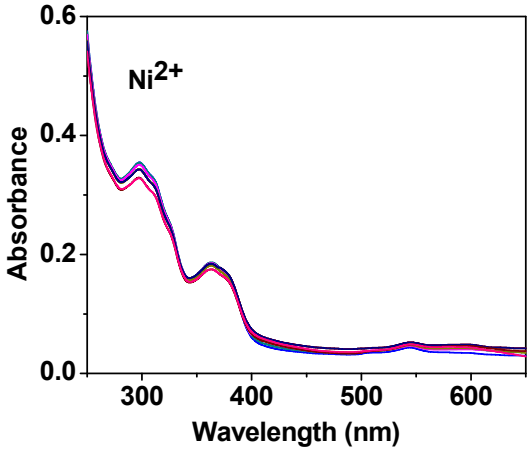
Ni2+
Absorbance
Wavelength (nm)
0.0
0.2
0.4
0.6
300
400
500
600

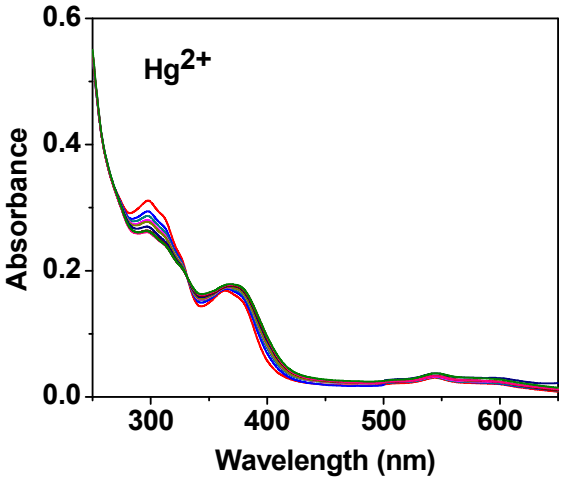
Hg2+
Absorbance
Wavelength (nm)
0.0
0.2
0.4
0.6
300
400
500
600

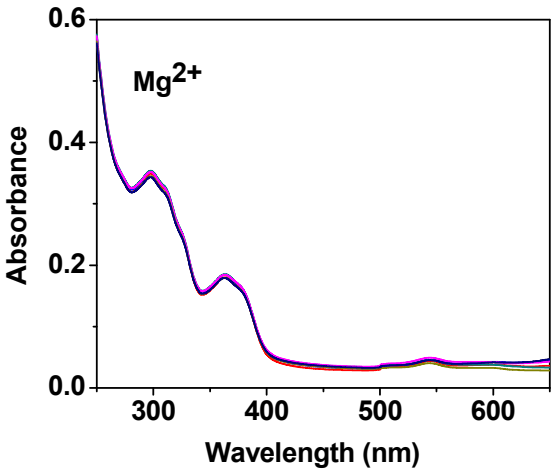
Mg2+
Absorbance
Wavelength (nm)
0.0
0.2
0.4
0.6
300
400
500
600

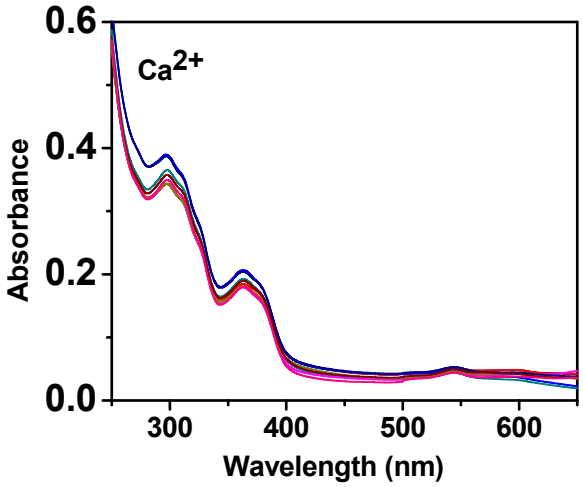
Ca2+
Absorbance
Wavelength (nm)
0.0
0.2
0.4
0.6
300
400
500
600

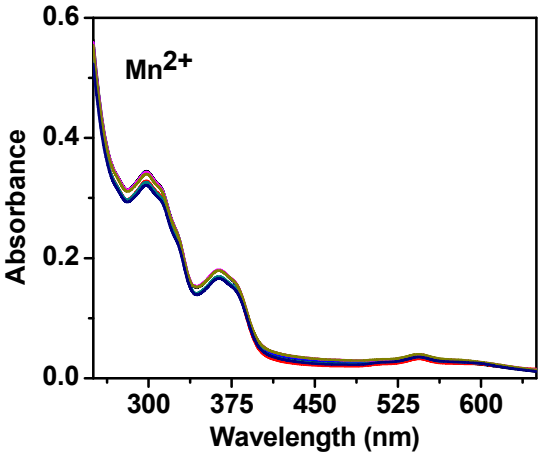
Mn2+
Absorbance
Wavelength (nm)
0.0
0.2
0.4
0.6
300
375
450
525
600

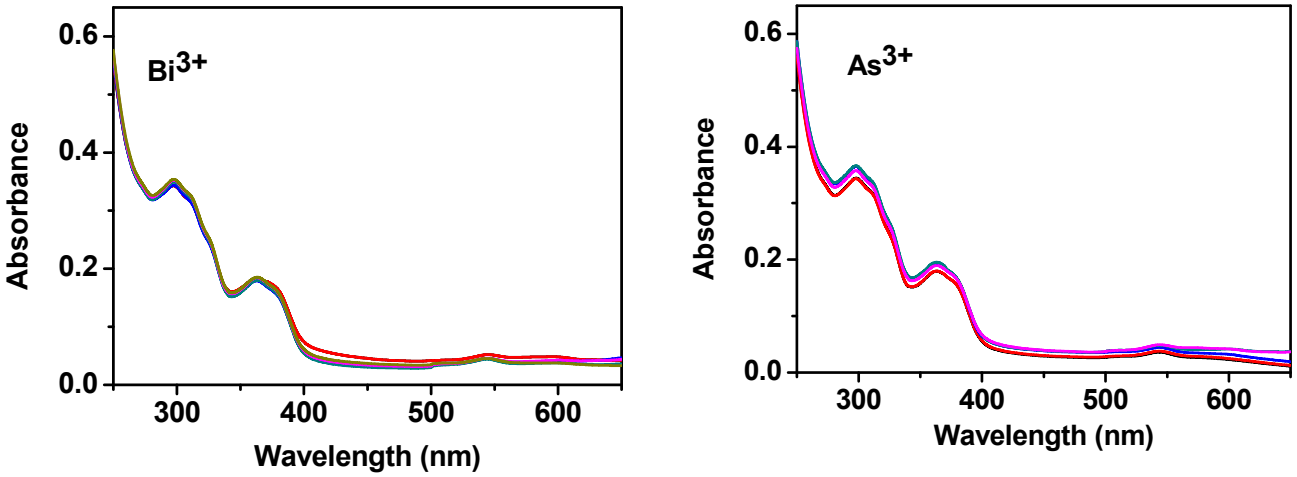

15. **References:**

1. (a) M. Shortreed, R. Kopelman, M. Kuhn, B. Hoyland *Anal. Chem.* 1996, **68**, 1414; (b) W. Lin, L. Yuan, Z. Cao, Y. Feng, L. Long *Chem. Eur. J.* 2009, **15**, 5096; (c) Y. Yang, T. Cheng, W. Zhu, Y. Xu, X. Qian *Org. Lett*. 2011, **13**, 264; (d) M. Zhu, M. Yuan, X. Liu, J. Xu, J. Lv, C. Huang, H. Liu, Y. Li, S. Wang, D. Zhu *Org. Lett*., 2008, **10**, 1481.

2. A.D. Becke, J. Chem. Phys. 98 (1993) 5648–5652.

3. C. Lee, W. Yang, R. G. Parr, Phys. Rev. B 37 (1988) 785–789.

4. D. Andrae, U. Haeussermann, M. Dolg, H. Stoll and H. Preuss, Theor. Chim. Acta 77 (1990) 123–141.

5. R. Bauernschmitt, R. Ahlrichs, Chem. Phys. Lett. 256 (1996) 454–464.

6. R.E. Stratmann, G.E. Scuseria, M.J. Frisch, J. Chem. Phys. 109 (1998) 8218–8224.

7. M.E. Casida, C. Jamorski, K.C. Casida, D.R. Salahub, J. Chem. Phys. 108 (1998) 4439–4449.

8. V. Barone, M. Cossi, J. Phys. Chem. A 102 (1998) 1995–2001.

9. M. Cossi, V. Barone, J. Chem. Phys. 115 (2001) 4708–4717.

10. M. Cossi, N. Rega, G. Scalmani, V. Barone, J. Comput. Chem. 24 (2003) 669–681.

11. Gaussian 03, Revision D.01, M. J. Frisch, G. W. Trucks, H. B. Schlegel, G. E. Scuseria, M. A. Robb, J. R. Cheeseman, J. A. Jr. Montgomery, T. Vreven, K. N. Kudin, J. C. Burant, J. M. Millam, S. S. Iyengar, J. Tomasi, V. Barone, B. Mennucci, M. Cossi, G. Scalmani, N. Rega, G. A. Petersson, H. Nakatsuji, M. Hada, M. Ehara, K. Toyota, R. Fukuda, J. Hasegawa, M. Ishida, T. Nakajima, Y. Honda, O. Kitao, H. Nakai, M. Klene, X. Li, J. E. Knox, H. P. Hratchian, J. B. Cross, V. Bakken, C.Adamo, J. Jaramillo, R. Gomperts, R. E. Stratmann, O. Yazyev, A. J. Austin, R. Cammi, C. Pomelli, J. W. Ochterski, P. Y. Ayala, K. Morokuma, G. A. Voth, P. Salvador, J. J. Dannenberg, V. G. Zakrzewski, S. Dapprich, A. D. Daniels, M. C. Strain, O. Farkas, D. K. Malick, A. D. Rabuck, K. Raghavachari, J. B. Foresman, J. V. Ortiz, Q. Cui, A. G. Baboul, S. Clifford, J. Cioslowski, B. B. Stefanov, G. Liu, A. Liashenko, P. Piskorz, I. Komaromi, R. L. Martin, D. J. Fox, T. Keith, M. A. Al-Laham, C. Y. Peng, A. Nanayakkara, M. Challacombe, P. M. W. Gill, B. Johnson, W. Chen, M. W. Wong, C. Gonzalez, and J. A. Pople, Gaussian, Inc., Wallingford CT, (2004).